

UNCLASSIFIED

AD NUMBER

ADB013340

LIMITATION CHANGES

TO:

Approved for public release; distribution is unlimited.

FROM:

Distribution authorized to U.S. Gov't. agencies only; Test and Evaluation; APR 1976. Other requests shall be referred to Air Force Armament Laboratory, Attn: DLJC, Eg;in AFB, 32542.

AUTHORITY

AFATL per ltr, 3 Jul 1979

THIS PAGE IS UNCLASSIFIED

THIS REPORT HAS BEEN DELIMITED
AND CLEARED FOR PUBLIC RELEASE
UNDER DOD DIRECTIVE 5200.20 AND
NO RESTRICTIONS ARE IMPOSED UPON
ITS USE AND DISCLOSURE.

DISTRIBUTION STATEMENT A

APPROVED FOR PUBLIC RELEASE;
DISTRIBUTION UNLIMITED.

2 60



AFATL-TR-76-47 ✓

ADB013340

**MUTUAL AERODYNAMIC INTERFERENCE EFFECTS
FOR MULTIPLE BODIES OF REVOLUTION
AND DISTORTED BODIES OF REVOLUTION**

See 915-7846

**DEPARTMENT OF AEROSPACE ENGINEERING
AUBURN UNIVERSITY
AUBURN, ALABAMA**

APRIL 1976

DDC
REFINED
SEP 14 1976
REGULATORY
C

FINAL REPORT: JUNE 1973 - SEPTEMBER 1975

AD NO.
DDC FILE COPY

Distribution limited to U. S. Government agencies only; this report documents test and evaluation; distribution limitation applied April 1976. Other requests for this document must be referred to the Air Force Armament Laboratory (DLJC), Eglin Air Force Base, Florida 32542.

AIR FORCE ARMAMENT LABORATORY

AIR FORCE SYSTEMS COMMAND • UNITED STATES AIR FORCE

EGLIN AIR FORCE BASE, FLORIDA



UNCLASSIFIED

SECURITY CLASSIFICATION OF THIS PAGE (When Data Entered)

19 REPORT DOCUMENTATION PAGE		READ INSTRUCTIONS BEFORE COMPLETING FORM
18 1. REPORT NUMBER AFATL-TR-76-47 ✓	2. GOVT ACCESSION NO.	3. RECIPIENT'S CATALOG NUMBER
6 4. TITLE (and Subtitle) Mutual Aerodynamic Interference Effects for Multiple Bodies of Revolution and Distorted Bodies of Revolution.	5. TYPE OF REPORT & PERIOD COVERED Final - June 1973 - September 1975	
	6. PERFORMING ORG. REPORT NUMBER	
10 7. AUTHOR(s) Fred W. Martin, Grady/Saunders, Jr. Malcolm A. Cutchins	15 8. CONTRACT OR GRANT NUMBER(s) F08635-71-C-0090 ✓ F08635-75-C-0023 new	
9. PERFORMING ORGANIZATION NAME AND ADDRESS Department of Aerospace Engineering Auburn University Auburn, Alabama	17 10. PROGRAM ELEMENT, PROJECT, TASK AREA & WORK UNIT NUMBERS 256702h 5 16 AF-2567	
11 11. CONTROLLING OFFICE NAME AND ADDRESS Air Force Armament Laboratory Armament Development and Test Center Eglin Air Force Base, Florida 32542	12. REPORT DATE Apr 1976	13. NUMBER OF PAGES 57
12 14. MONITORING AGENCY NAME & ADDRESS (if different from Controlling Office) 57p.	15. SECURITY CLASS. (of this report) UNCLASSIFIED	
15a. DECLASSIFICATION/DOWNGRADING SCHEDULE		
16. DISTRIBUTION STATEMENT (of this Report) 9 Final rept. Jun 73-Sep 75,		
17. DISTRIBUTION STATEMENT (of the abstract entered in Block 20, if different from Report) Distribution limited to U.S. Government agencies only; this report documents test and evaluation; distribution limitation applied April 1976. Other requests for this document must be referred to the Air Force Armament Laboratory, DLJC, Eglin Air Force Base, Florida 32542.		
18. SUPPLEMENTARY NOTES Available in DDC		
19. KEY WORDS (Continue on reverse side if necessary and identify by block number) Aerodynamic Interference Multiple Bodies of Revolution Distorted Bodies of Revolution Mutual Interference		
20. ABSTRACT (Continue on reverse side if necessary and identify by block number) A method of solution for the aerodynamic flow field about two bodies at angle of attack including mutual interference effects has been devised for bodies with circular cross-section. The analytical method used is a modification of a method of solution for the flow about axisymmetric bodies in close proximity at zero angle of attack. As a demonstration of this method, the flows about one, two and three finless M-117 bomb shapes were investigated. Theoretical pressure distributions are presented for the two and three body cases. For the three body case, experimental data is available; however, there is poor agreement with data		

DD FORM 1 JAN 73 1473 EDITION OF 1 NOV 65 IS OBSOLETE

401926 UNCLASSIFIED

SECURITY CLASSIFICATION OF THIS PAGE (When Data Entered)

UNCLASSIFIED

SECURITY CLASSIFICATION OF THIS PAGE(When Data Entered)

20. (Continued)

thought primarily to be because of flow separation along the tails of the bombs. A non-axisymmetric modification of the M-117 bomb shape was developed in order to simulate the flow separation. The analytical results of this effort are compared with the experimental data.

ADDITION 1st	
HTB	Write Section <input type="checkbox"/>
908	Diff Section <input checked="" type="checkbox"/>
UNCLASSIFIED	<input type="checkbox"/>
JUSTIFICATION	
BY	
AUTHORITY AVAILABILITY CODES	
Doc	A 111 218, 7 SPECIAL
B	

UNCLASSIFIED

PREFACE

The work described in this report was done during the period from June 1973 through June 1974 under Contract Number F08635-71-C-0090 with the Air Force Armament Laboratory, Eglin Air Force Base, Florida, and modified during September 1974 through September 1975 under Contract Number F08635-75-C-0023, and forms some of the basis for the current effort under Contract Number F08635-76-C-0079. The original Program Manager was Captain Visi Arais (DLJC), who was followed by Lieutenant Norman Speakman (DLJC), while the present Program Manager is Captain Robert Grow (DLJC). This work is a follow-up effort of the work reported as AFATL-TR-73-161, Mutual Aerodynamic Interference Effects for Two Axisymmetric Bodies, dated August 1973.

This technical report has been reviewed and is approved for publication.

FOR THE COMMANDER



WILLIAM F. BROCKMAN, Colonel, USAF
Chief, Munitions Division

TABLE OF CONTENTS

Section	Title	Page
I	INTRODUCTION	1
II	THEORETICAL CONSIDERATIONS	2
	Introduction	2
	Discussion of Body Geometry.	3
	Single Body Solution	3
	Axisymmetric Considerations.	3
	Cross-Flow Considerations.	5
	Two Body Solution.	6
	Source-Sink Image Solution	6
	Doublet Image Solution	8
	Multiple Body Solution	15
III	NUMERICAL EXAMPLES	19
	Single Body.	19
	Two Parallel Bodies.	25
	Three Bodies	25
IV	CONCLUSIONS	36
APPENDIX A	Influence Coefficients.	37
APPENDIX B	Image System for Two Circular Cross-Sections in Two-Dimensional Flow	42
REFERENCES	47
LIST OF SYMBOLS	49

LIST OF FIGURES

Figure	Title	Page
1	Typical Non-Axisymmetric Body Derived from an Axisymmetric Body	4
2	Example of Geometry of Y_o , R_a , and R_b	7
3	Image of a Doublet in a Circle	10
4	Partial Image System for a Doublet and Two Circles.	11
5	Partial Image System for Two Circles with Doublets at Both Centers	12
6	Example of Control Points Used for Solution of Image Doublet Strengths	16
7	Representative Cross-Section of Three Bodies.	17
8	Profiles of M-117 Bomb Shape	20
9	Single and Multiple Body Configurations	21
10	Pressure Distribution - Single Body at 0-Degree Angle of Attack	22
11	Pressure Distribution - Single Body at 5-Degree Angle of Attack	23
12	Pitching Moment Coefficient - Single Body	24
13	Pressure Distribution - Two Bodies at 0-Degree Angle of Attack ($\theta = 180^\circ$).	27
14	Pressure Distribution - Two Bodies at 0-Degree Angle of Attack ($\theta = 0^\circ$)	28
15	Comparison of the Analytical Pressure Distribution for Two Bodies at 0 and 5-Degree Angle of Attack	29
16	Side Force Coefficient - Two Body Configuration	31
17	Pitching Moment Coefficient - Two Body Configuration	32
18	Boundary Condition Error Distribution - Two Bodies ($\theta = 0^\circ$) . .	33
19	Pressure Distribution - Three Axisymmetric Bodies ($\theta = 90^\circ$) . .	34

LIST OF FIGURES (CONCLUDED)

Figure	Title	Page
20	Pressure Distribution - Three Modified Non-Axisymmetric Bodies ($\theta = 90^\circ$).	35
A-1	Transformation of Induced Velocities.	38
B-1	Two-Dimensional Representation of a Cross-Section of Two Bodies (without image system)	43
B-2	Two Circles with the First Iteration of Image System	44
B-3	Two Circles with Third Iteration of Image System.	45

(The reverse of this page is blank)

SECTION I

INTRODUCTION

A concise mathematical model for the representation of the flow about two or more axisymmetric bodies at zero angle of attack in irrotational, incompressible flow has been presented by Martin (Reference 1,2). The purpose of this investigation is to modify their method to take into account free stream cross-flow due to angle of attack and to allow the consideration of slightly non-axisymmetric bodies.

The method, as given in Reference 2, consists of distributing a set of point sources along the axis of each body which represents that body in an isolated flow situation, and then adding to this a set of source-sink pairs that preserves the body shapes when the bodies are brought into close proximity. The method discussed herein retains the system of sources and source-sink pairs, but adds to it a system of doublets that accounts for both the freestream cross-flow due to angle of attack and the flow due to distortion of the body centerlines.

The new technique was applied to calculate the flow field about one, two, and three M-117 stores. The results of these calculations are presented in Section III.

SECTION II

THEORETICAL CONSIDERATIONS

INTRODUCTION

This report documents the derivation and evaluation of a method of mathematically modeling the flow around two or more bodies in close proximity in irrotational, incompressible flow. The restriction is made that the bodies are either axisymmetric bodies of revolution, or bodies which are derived from a body of revolution by warping, or curving, the centerline. Also, the angle of attack of the bodies must be small.

The governing equation of the flow as described is the Laplace equation and can be expressed as

$$\nabla^2 \phi = 0 \quad (1)$$

with the usual body boundary condition expressed by

$$\bar{V} \cdot \text{grad}(f) = 0 \quad (2)$$

Note that $f(x,y,z) = 0$ is the equation of the body. Since Equation (1) is linear, the method of superposition can be used. Therefore, the solution as given in Reference 2 for mutual aerodynamic interference of two similar and aligned axisymmetric bodies can be extended to include a greater number of bodies. Also, by the addition of doublets and their images, the effects of freestream cross-flow can be taken into account. This method assumes that the mutual interference effects of the bodies will be such that the effects of any shed vortices as discussed in Reference 3 can be neglected.

The multiple body solution is generated in four basic steps as follows:

1. For each body a set of point sources is distributed along the centerline. Their strengths are determined so that the body boundary conditions are satisfied treating the body as an axisymmetric body aligned in a flow with a velocity equal to the axial component of the freestream. This set of point sources will be referred to as the single body sources.
2. Next, for each body a set of doublets is found which, combined with the single body sources, represents the actual body shape. This includes both the warped body effects and the freestream cross-flow due to angle of attack.

3. In the third step, a set of image source-sink pairs for each body are found for each possible combination of bodies taken a pair at a time. This step is similar to the method as given in Reference 2, but takes into account the warp of the bodies.

4. Finally, sets of image doublets are found for each unique pair of bodies. The body boundary conditions used in this analysis take into account the flow field generated by all sources, image pairs, and doublets which were previously found for the two bodies of the pair.

DISCUSSION OF BODY GEOMETRY

A basic body of revolution is geometrically described in three dimensional space by expressing the local body radius, R , as a function of axial position, x . That is, R is an explicit function of x where x is measured along the axis of revolution from nose to tail as shown in Figure 1(a). The non-axisymmetric bodies used in this work are obtained by taking the body of revolution and distorting it by warping the axis, as shown in Figure 1(b), while the local cross-section taken perpendicular to the new axis remains circular and of the same radius and slope relative to the centerline as the cross-section at the corresponding station of the unwarped body. In order to define the distorted body geometry, variables are introduced which define the centerline displacement R_w , the meridional direction of the displacement ϕ_w , and the angular rotation of the radius vector from its original position ψ_w . For simplicity, the restriction is made that the warpage of the body centerline lies in one plane; therefore, the meridional direction of the displacement ϕ_w is the same along the length of the body.

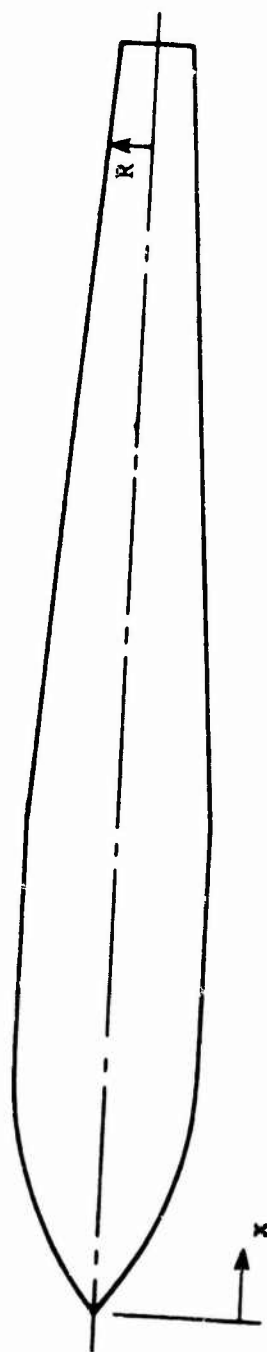
SINGLE BODY SOLUTION

The representation of the flow about a single isolated body at angle of attack is accomplished by superimposing the axisymmetric solution and the cross-flow solution. Details of this analysis are discussed in the following sections.

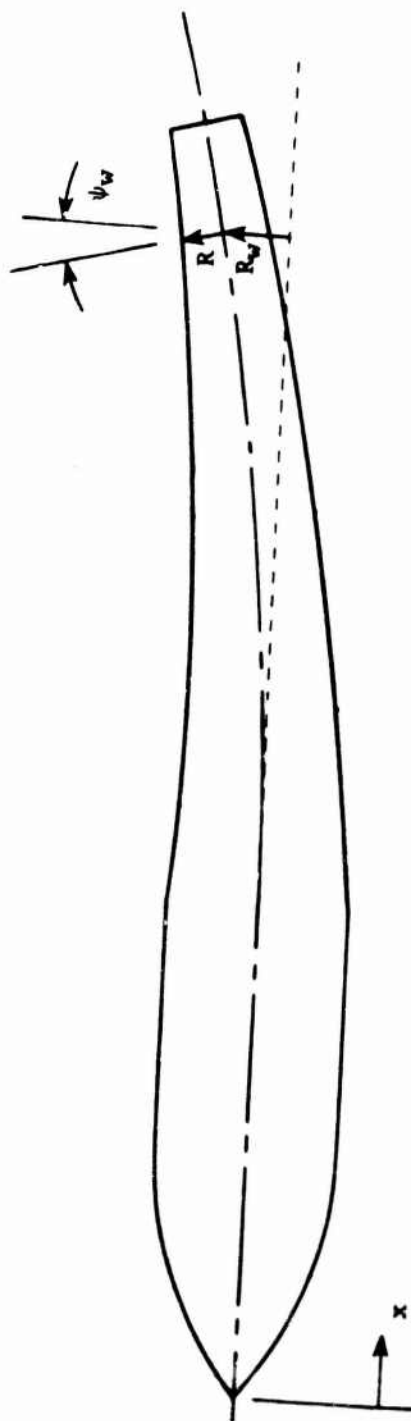
Axisymmetric Considerations

Since the axis of the body is not necessarily aligned with the flow, only the component of freestream velocity in the axial direction of the body is used for the axisymmetric solution. The solution technique, as given in detail in Reference 2, consists of distributing a number of point sources along the body axis at equally spaced intervals and finding their strengths by simultaneous solutions such that the body boundary condition relating the velocity with the slope, S , of the body surface is satisfied. The mathematical expression of this boundary condition is

$$\frac{U_{r_s}}{U_{x_\infty} + U_{x_s}} = S \quad (3)$$



(a) Axisymmetric Body



(b) Non-axisymmetric

Figure 1. Typical Non-axisymmetric Body Derived from an Axisymmetric Body

Rearranging Equation (3) (and using the influence coefficients for sources derived in Appendix A), the boundary condition equation for N_s sources can be expressed as

$$\sum_{i=1}^{N_s} \{ (C_{r_{s_i}} - C_{x_{s_i}} S) m_i \} = S U_{x_\infty} \quad (4)$$

Equation (4) is applied at N_s control points on the body surface and yields N_s equations for the simultaneous solution of the N_s unknown source strengths. Since the flow is axisymmetric, the meridional plane in which the control points lie is irrelevant and the boundary condition is satisfied all around the body. It has been found, however, that the control points should be taken at the same axial station as the point sources for best agreement of experiment and theory.

Cross-Flow Considerations

The cross-flow solution consists of a set of doublets needed to satisfy the body boundary conditions due to the cross-flow. In the case of the warped body, the cross-flow at each cross-section of the body is defined as the component of the freestream velocity that is normal to the local body axis (i.e., the component that lies in the cross-sectional plane). For either the axisymmetric or warped body cases, the axial velocity component (U_{x_∞}) is defined as the freestream velocity component parallel to the local body axis (i.e., normal to the cross-sectional plane).

A doublet is located at each of the N_s stations coincident in location with the single body source at that station. The axis of the doublet lies in the cross-sectional plane and is aligned with the freestream cross-flow velocity component. The boundary condition for the solution of the required strengths of the doublets is to require that at the control points on the body surface, the sum of all induced velocities and freestream velocities is tangent to the body surface. This can be expressed as

$$\frac{U_{r_\infty} + U_{r_s} + U_{r_d}}{U_{r_\infty} + U_{x_s} + U_{x_d}} = S \quad (5)$$

Rearranging Equation (5) yields

$$U_{r_d} - U_{x_d} S = (U_{x_\infty} + U_{x_s}) S - (U_{r_\infty} + U_{r_s}) \quad (6)$$

which can be rewritten in terms of velocity influence coefficients to yield

$$\sum_{i=1}^{N_s} \{ (C_{r_{d_i}} - C_{x_{d_i}} S) u_i \} = (U_{x_\infty} + U_{x_s}) S - (U_{r_\infty} + U_{r_s}) \quad (7)$$

Applying Equation (7) to N_s control points on the body yields the necessary number of simultaneous equations for the solution of the doublet strengths. To avoid exaggeration of the doublet strengths, the control points for their solution are located such that the effect of the doublets on the radial velocity at the control points is maximized. Therefore, the control points are located at the intersections of the doublet axes and the body surface.

TWO BODY SOLUTION

The purpose of the two body solution is to find a set of source-sink pairs and a set of doublets in each of the two bodies that will preserve the body shapes when the two bodies are in close proximity. These are called the image source-sink pairs and image doublets, respectively. The first step is the solution of the image source-sink pairs while ignoring the effects of the single body doublets and freestream cross-flow. This solution is a modification of the two body solution for two similar aligned bodies which was done in the work described in Reference 2. The two-dimensional Milne-Thomson (Reference 4) circle theorem (see Appendix B) is used to determine the geometry for the image system of three-dimensional source-sink pairs that are located at each station of the bodies.

Source-Sink Image Solution

As indicated by the circle theorem, the sink of the source-sink pair at each station is located on the axis (coinciding with the location of the single body source at that station) while the source is displaced a distance, δ , perpendicular to the axis in the direction of the other body. The magnitude of δ , as derived in Appendix B, is given by the equation

$$\delta = \frac{Y_o - \frac{(R_a^2 - R_b^2)}{Y_o}}{2} - \left\{ \frac{\left[Y_o - \frac{(R_a^2 - R_b^2)}{Y_o} \right]^2}{4} - R_a^2 \right\}^{1/2} \quad (8)$$

where the geometric variables are shown in Figure 2.

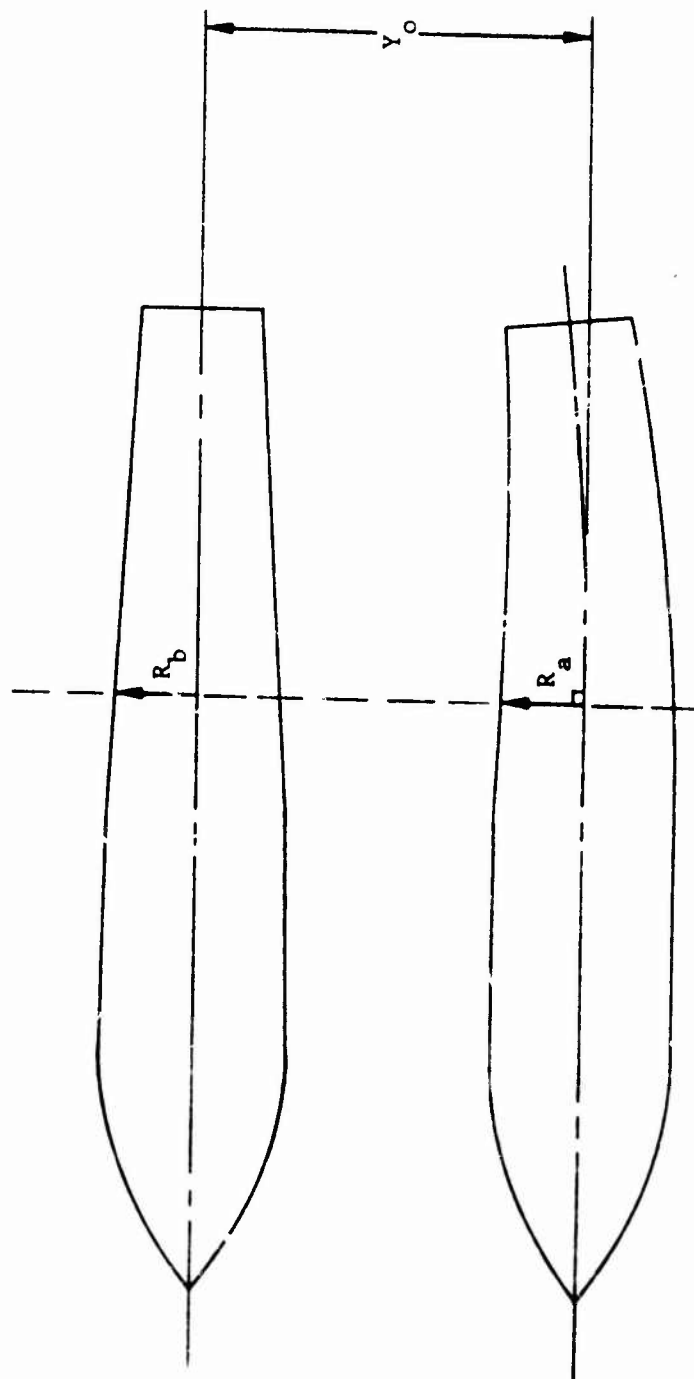


Figure 2. Example of Geometry of Y_o , R_a and R_b .

The strengths of the $2N_s$ image-pairs (N_s in each body) are found by the solution of $2N_s$ simultaneous equations using the tangent flow boundary condition which is applied at a control point on the body surface at each station of the two bodies. The control point at each station is selected such that it is colinear with the source and sink of the image pair. The mathematical expression for the boundary condition is

$$\frac{U_{r_s} + U_{r_p}}{U_{x_\infty} + U_{x_s} + U_{x_p}} = S \quad (9)$$

Rearranging Equation (9) yields

$$U_{r_p} - U_{x_p} S = (U_{x_\infty} + U_{x_s}) S - U_{r_s} \quad (10)$$

Using the velocity influence coefficients as derived in Appendix A, Equation (10) becomes

$$\begin{aligned} & \sum_{k=1}^2 \sum_{i=1}^{N_s} \{ (C_{r_{s_{ik}}}^+ - C_{x_{s_{ik}}}^+ S) m_{ik} + (C_{r_{s_{ik}}}^- - C_{x_{s_{ik}}}^- S)(-m_{ik}) \} \\ & = (U_{x_\infty} + U_{x_s}) S - U_{r_s} \end{aligned} \quad (11)$$

Rearranging Equation (11) yields

$$\begin{aligned} & \sum_{k=1}^2 \sum_{i=1}^{N_s} \{ (C_{r_{s_{ik}}}^+ - C_{r_{s_{ik}}}^- - (C_{x_{s_{ik}}}^+ - C_{x_{s_{ik}}}^-) S) m_{ik} \} \\ & = (U_{x_\infty} + U_{x_s}) S - U_{r_s} \end{aligned} \quad (12)$$

Applying Equation (12) to the control points at each station of both bodies yields the required number of equations ($2N_s$) discussed previously.

Doublet Image Solution

An image system must be derived that will preserve the body shapes when the effects of the doublets of both bodies are included. Again the two-dimensional approach is taken. The image system that creates a circular streamline in the flow field of a two-dimensional doublet is

derived in Section 8.81 of Reference 4. The system consists of a doublet located a distance a^2/f from the center of the circle on the line connecting the center of the circle and the original doublet (See Figure 3). The orientation of the image doublet is such that its axis is antiparallel to the axis of the original doublet. The strength of the image doublet, μ' , is given by

$$\mu' = \mu \left[\frac{a}{f} \right]^2 \quad (13)$$

If an additional circle that is centered about the original doublet is considered, then an image doublet is needed therein to counteract the effects of the image doublet in the first circle (the effects of the original doublet on the second circle do not need to be considered since they are necessary to counteract the freestream cross-flow). Conversely, another image doublet is needed in the first circle due to the effects of the image in the second, and so on until a limiting condition is met (See Figure 4).

The magnitudes of the image doublet displacements follow the same series of mathematical expressions as that of the source of the image source-sink pairs, with the limiting displacement for the infinite iteration given by Equation (8). Thus, the image system for two circles with one centered about a doublet consists of an infinite number of image doublets in both circles. The doublets, in the circle that does not enclose the original doublet, will all have the same orientation (antiparallel to the original doublet) and will be displaced from the circle center by amounts ranging from the initial image location a^2/f to the limiting value δ_a given as

$$\delta_a = \frac{f - \frac{b^2 - a^2}{f}}{2} - \left\{ \frac{\left[f - \frac{b^2 - a^2}{f} \right]^2}{4} - a^2 \right\}^{1/2} \quad (14)$$

The image doublets, in the circle that is centered about the original doublet, will all have an orientation that is parallel to the original doublet and will be displaced by amounts ranging from $b^2/(f - a^2/f)$ as shown in Figure 4 to the limiting value δ_b given as

$$\delta_b = \frac{f - \frac{a^2 - b^2}{f}}{2} - \left\{ \frac{\left[f - \frac{a^2 - b^2}{f} \right]^2}{4} - b^2 \right\}^{1/2} \quad (15)$$

If an additional doublet is considered that is located in the first circle, then an additional set of an infinite number of image doublets are needed in both circles (See Figure 5).

For simplification, one image doublet is used in each cross-section to approximate the infinite number of doublets suggested by the two-dimensional analysis. This cross-sectional location of the doublet was

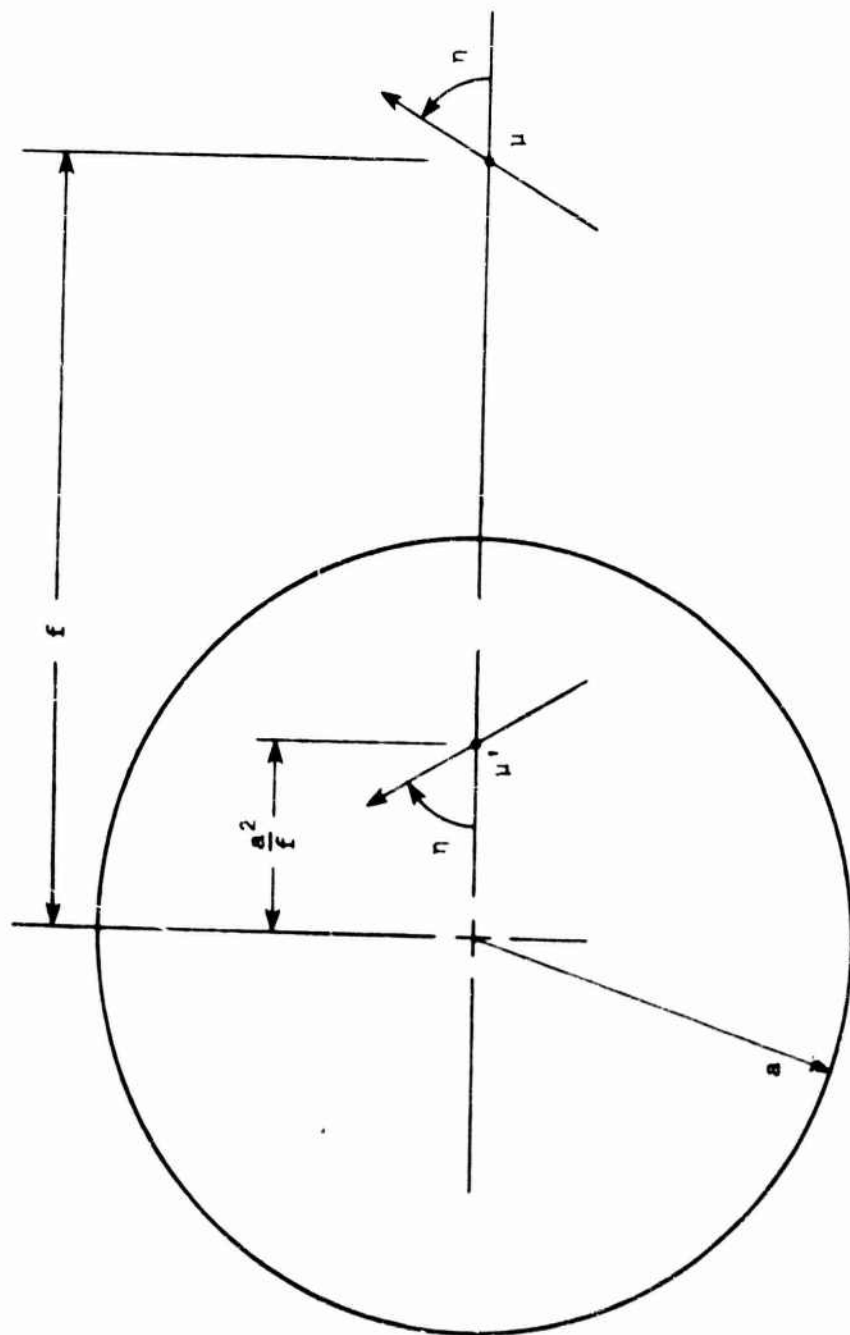


Figure 3. Image of a Doublet in a Circle

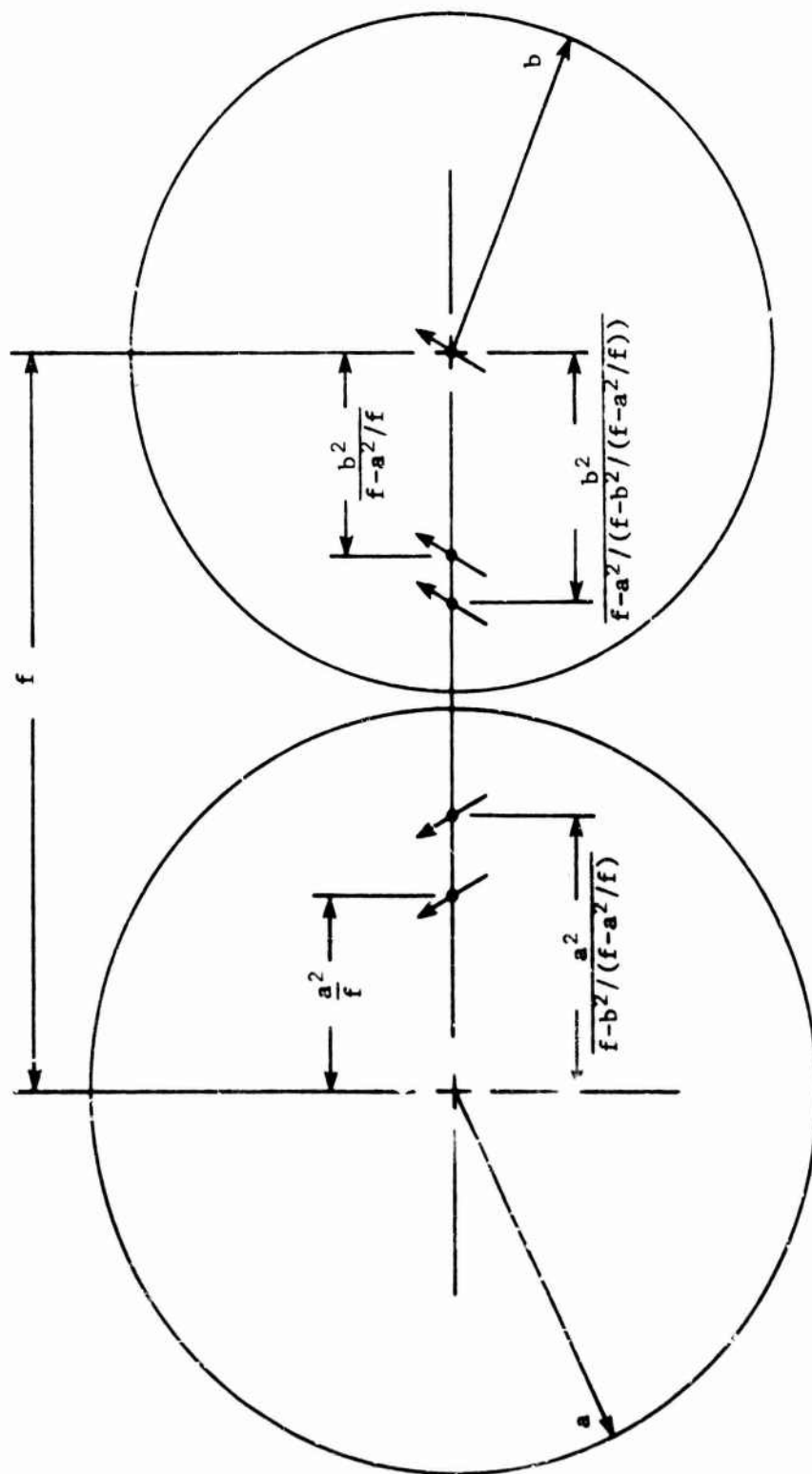


Figure 4. Partial Image System for a Doublet and Two Circles

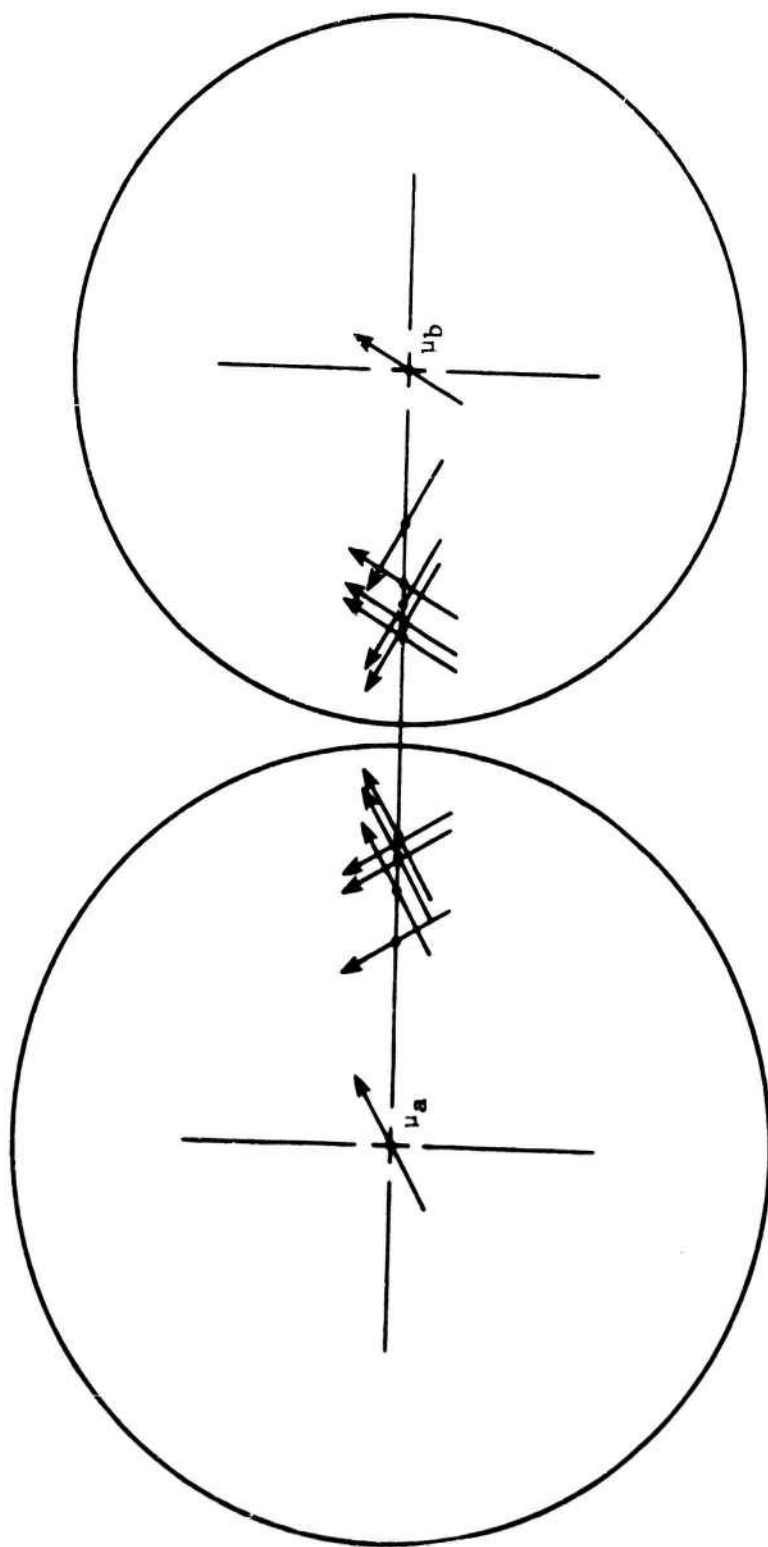


Figure 5. Partial Image System for Two Circles with Doublets at Both Centers

chosen by computational experimentation as the midpoint between the first and third order terms; that is, between a^2/f and $a^2/(f-b^2/(f-a^2/f))$. The orientation of the image doublet is given by the vector sum of the first and second order image terms in that cross-section. This is justified by use of the complex potential for doublets in two-dimensional flow. The general complex potential for a doublet as derived in Section 8.23 of Reference 4 is

$$w = \frac{\mu e^{i\eta}}{Z-Z_0} \quad (16)$$

Therefore, if a single doublet is used to represent two doublets that are located at the same point but have different strength and orientations, then the relationship between the complex potentials must be:

$$\frac{\mu_3 e^{i\eta_3}}{Z-Z_0} = \frac{\mu_1 e^{i\eta_1}}{Z-Z_0} + \frac{\mu_2 e^{i\eta_2}}{Z-Z_0} \quad (17)$$

Multiplying through by $Z-Z_0$ and writing the results in the form of cosines and sines, gives

$$\begin{aligned} \mu_3(\cos \eta_3 + i \sin \eta_3) \\ = \mu_1(\cos \eta_1 + i \sin \eta_1) + \mu_2(\cos \eta_2 + i \sin \eta_2) \end{aligned} \quad (18)$$

By setting the real and imaginary parts equal, Equation (18) yields the following simultaneous equations

$$\mu_3 \cos \eta_3 = \mu_1 \cos \eta_1 + \mu_2 \cos \eta_2 \quad (19a)$$

$$\mu_3 \sin \eta_3 = \mu_1 \sin \eta_1 + \mu_2 \sin \eta_2 \quad (19b)$$

Dividing Equation (19a) into (19b) yields

$$\tan \eta_3 = \frac{\mu_1 \sin \eta_1 + \mu_2 \sin \eta_2}{\mu_1 \cos \eta_1 + \mu_2 \cos \eta_2} \quad (20)$$

Therefore, η_3 is the orientation of the results of the vectorial addition of the complex vectors $\mu_1 e^{i\eta_1}$ and $\mu_2 e^{i\eta_2}$.

Applying Equation (20) to the combination of the first and second image doublets yields

$$\tan \eta_{\delta} = \frac{\{\mu_b' \sin(\pi - \eta_b) + \mu_a'' \sin \eta_a\}}{\{\mu_b' \cos(\pi - \eta_b) + \mu_a'' \cos \eta_a\}} \quad (21)$$

The strengths of the first and reflected image doublets, μ_b' and μ_a'' , respectively, are given by the two-dimensional analysis as

$$\mu_b' = \left[\frac{a}{f} \right]^2 \mu_b \quad (22a)$$

and

$$\mu_a'' = \left[\frac{b}{f} \right]^2 \left[\frac{a}{f-b^2} \right]^2 \mu_a \quad (22b)$$

The two-dimensional analysis for the image doublets is applied to the three-dimensional flow problem in the same fashion as the application of the two-dimensional analysis for the sources, where R_a , R_b and Y_0 correspond to a , b , and f , respectively. By these means, there is an image doublet located in the cross-section at each of the N_s stations of both bodies.

The strengths of the image doublets are found by using the tangent flow boundary condition which is now expressed as

$$\frac{U_{r_{\infty}} + U_{r_s} + U_{r_p} + U_{r_d} + U_{r_{\delta}}}{U_{x_{\infty}} + U_{x_s} + U_{x_p} + U_{x_d} + U_{x_{\delta}}} = S \quad (23)$$

Rearranging Equation (23) yields

$$U_{r_{\delta}} - U_{x_{\delta}} S = (U_{x_{\infty}} + U_{x_s} + U_{x_p} + U_{x_d}) S - (U_{r_{\infty}} + U_{r_s} + U_{r_p} + U_{r_d}) \quad (24)$$

Expressing Equation (24) in terms of influence coefficients of the doublets, gives

$$\begin{aligned} \sum_{k=1}^2 \sum_{i=1}^{N_s} \{C_{r_{\delta} ik} - C_{x_{\delta} ik} S\} \mu_{ik} &= (U_{x_{\infty}} + U_{x_s} + U_{x_p} + U_{x_d}) S \\ &\quad - (U_{r_{\infty}} + U_{r_s} + U_{r_p} + U_{r_d}) \end{aligned} \quad (25)$$

To avoid exaggeration of the doublet strengths, it is desirable to locate the control points for their solution such that the effect of the doublets on the radial velocity at the control points is maximized. This dictates that a control point is located at the cross-section in which each doublet lies. Furthermore, it is desired that the meridional location of the control point for a given cross-section should maximize the radial velocity induced at the control point by the doublet in that cross-section. However, the calculations required to find this location are excessive and to save computer time an alternate location is used. The location used is the closest (to the doublet) of the two intersections of the doublet axis and the body surface. This control point is shown for a representative cross-section in Figure 6. This location insures that the doublet will have a strong effect at the control point even though the effect is not maximized.

MULTIPLE BODY SOLUTION

The representation of a multiple body interference flow field is accomplished by executing the single body solution for each body, then executing the two body-solution for each body pair in turn, and finally, combining the results. As an illustration of this combination, a representative cross-section of three bodies is shown in Figure 7. Points a, b, and c represent the single body doublets of the three bodies. The orientation of the doublets and the single body sources that are also a result of the single body solution are not shown for clarity. Points ab and ba represent the locations of the image doublets that are created by the execution of the two-body solution for Bodies A and B. Again, for clarity, the doublet axes and the image source-sink pairs that are also a result of the two-body solution are not shown. Similarly, points ac and ca represent the locations of the images created by the two-body solution of Bodies A and C and points bc and cb represent the locations of the images created by the two-body solution of Bodies B and C.

By combining the results of all the two-body solutions, there are image systems in each body that prevent that body's shape from being distorted by the single body sources and doublets of the other bodies. This does not, however, prevent the body shape from being distorted by the image systems of the other bodies. To illustrate this, Body A in Figure 7 is used as an example. The image systems created by the two-body solution of Bodies A and B (partially represented by points ab and ba) prevent the distortion of Body A by the single body sources and doublets of Body B and also prevent the distortion of Body B by the single body sources and doublets of Body A. Similarly, the image systems created by the two-body solution of Bodies A and C (represented by points ac and ca) prevent mutual distortion of the shapes of Bodies A and C. The image systems presented thus far are required in order to prevent the distortion of the shape of Body A by the single body sources and doublets of Bodies B and C. However, the image systems that are created by the two-body solution of Bodies B and C are also included in the flow field. Hence, an additional image system is needed in Body A (partially

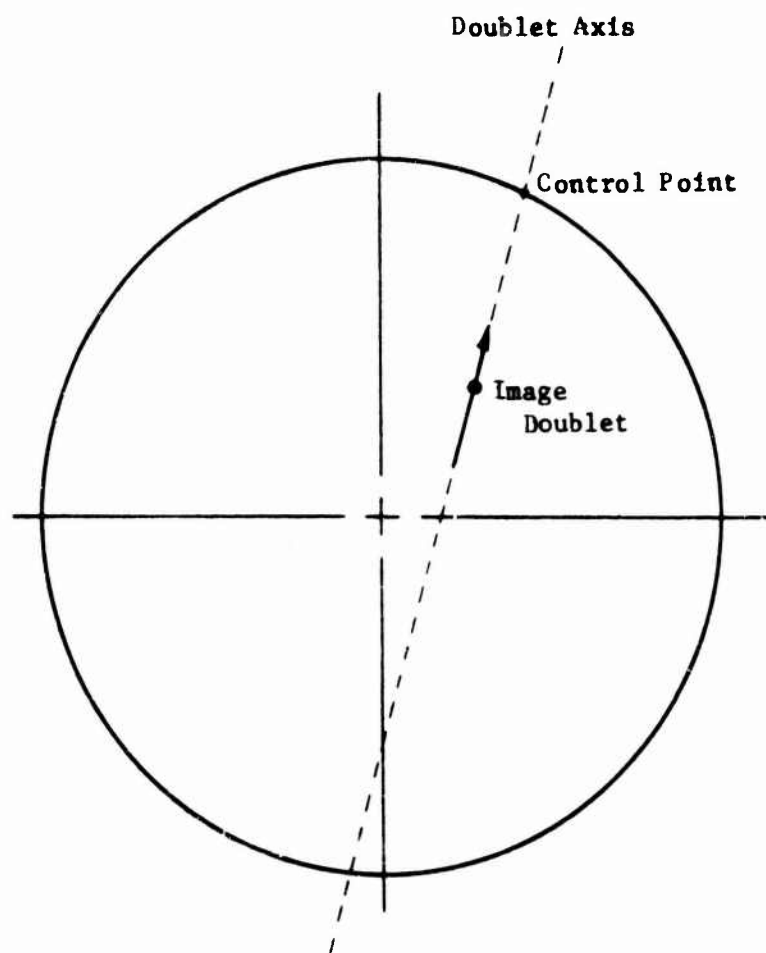
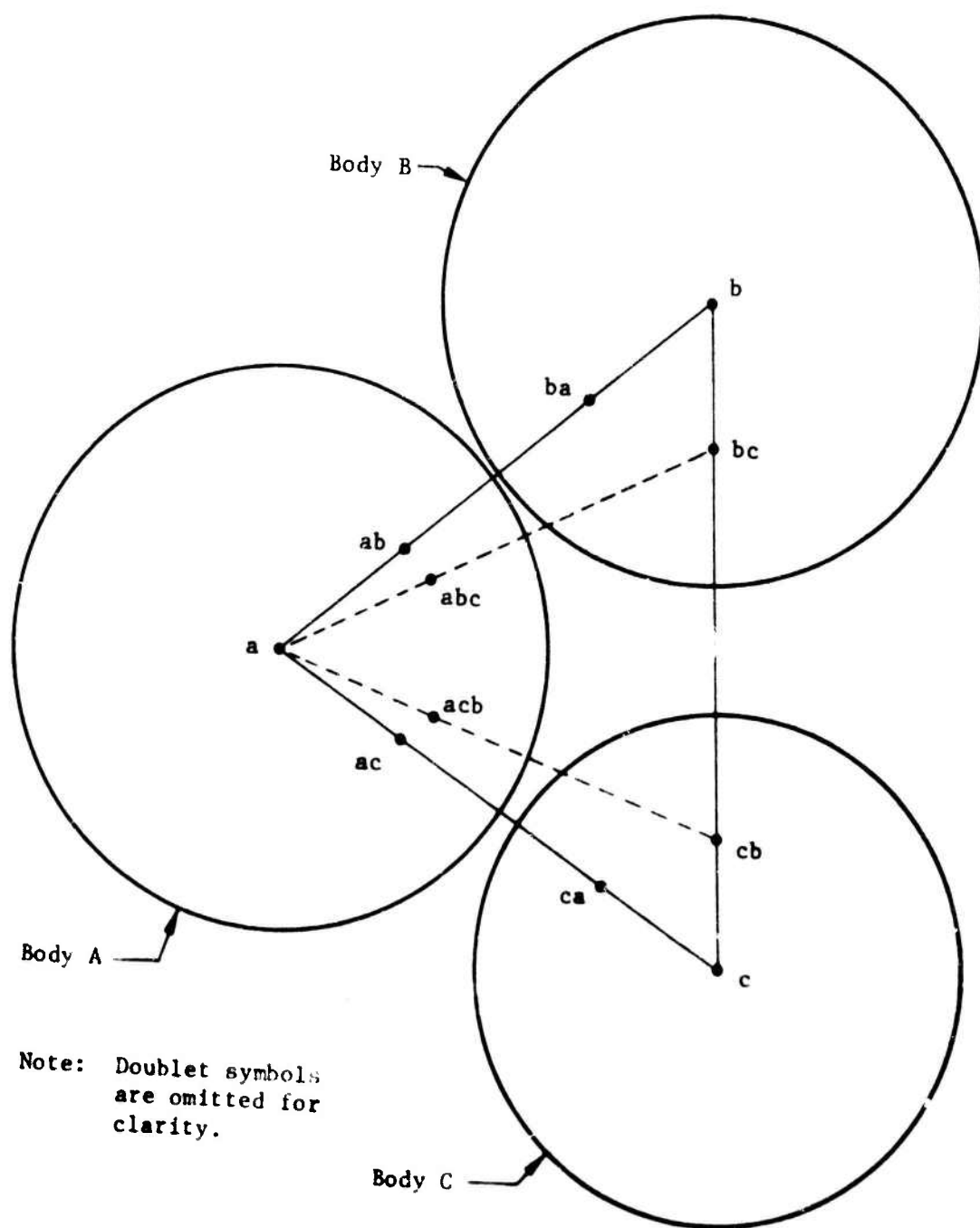


Figure 6. Example of Control Points Used for Solution of Image Doublet Strengths



Note: Doublet symbols
are omitted for
clarity.

Figure 7. Representative Cross-Section of Three Bodies

represented by points abc and acb) to prevent distortion by the image source-sink pairs and image doublets resulting from the two-body solution of Bodies B and C. A similar situation exists for Body B and for Body C due to the two-body solutions of Bodies A and C and Bodies A and B, respectively. It has been found, however, that the contribution of these higher order image terms is at best an order of magnitude less significant than the two-body image system. Therefore, since these terms have little effect on the solution, as can be shown by the fact that the distortion of the body shapes is small when only the results of the single body and two-body solutions are added, the higher order image terms are neglected.

SECTION III

NUMERICAL EXAMPLES

The numerical examples presented here are based on the M-117 bomb shape (without fins) which is shown in Figure 8.(a). The geometry of the M-117 bomb can be described in three axial intervals. They are the nose section, the center section, and the tail section. The nose section is of ogival shape (circular arc) with a length to maximum diameter ratio of 1.32. The center section is a circular cylinder with a length of 1.22 diameters. The tail section is a straight taper of 7.5 degrees and terminates in a boattail. The length of the actual M-117 tail is 2.96 diameters; however, a length of 3.47 diameters is used in these examples to give some allowance for flow separation at the truncated boattail.

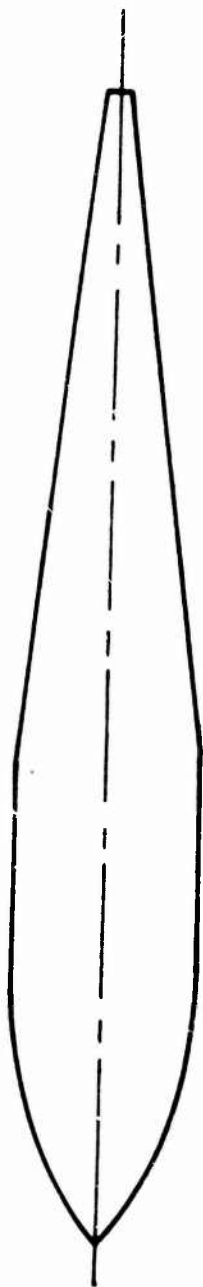
All theoretical data presented in this section were obtained by the use of a Fortran Computer Program. The pressure coefficients along the body surface were calculated for 24 evenly spaced meridional planes. Force and moment coefficients were then calculated by numerically integrating the pressure coefficients. The reference area and length used for the coefficients are, respectively, the maximum cross-sectional area and the diameter of the M-117 bomb. The moment coefficients are referred to the center of gravity which is 2.05 bomb diameters from the nose. To aid in the evaluation of the modeling technique, error calculations were made at each station around the body by finding the flow angle (with respect to the body centerline) created by all induced and freestream velocities and subtracting the angle of the body surface.

The configurations used for the numerical examples are shown in Figure 9. They are drawn as though the viewer were looking downstream at the nose of the bodies. The arrows indicate the direction of the freestream cross-flow due to angle of attack.

SINGLE BODY

The case of a single M-117 bomb aligned with the flow has been previously treated in Reference 2, and the resulting pressure distribution has been found to be in good agreement with experimental data obtained in the low speed wind tunnel at the contractor's as shown in Figure 10. Figure 11 shows the pressure distributions along the leeward and windward meridional planes for a M-117 bomb at 5 degrees angle of attack.

The analytical force and moment coefficients for the isolated body were found to be negligible except for the pitching moment which is plotted in Figure 12 for angles of attack ranging from zero to 10 degrees.

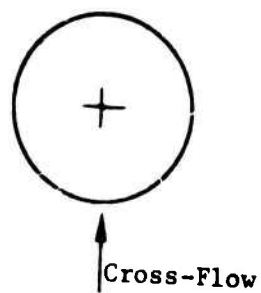


(a) Axisymmetric

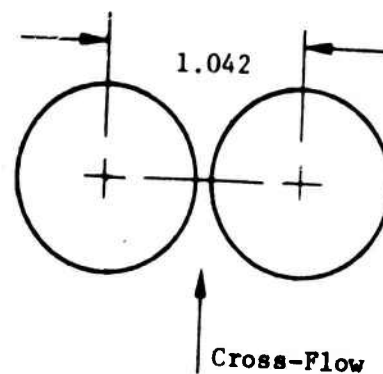


(b) Modified

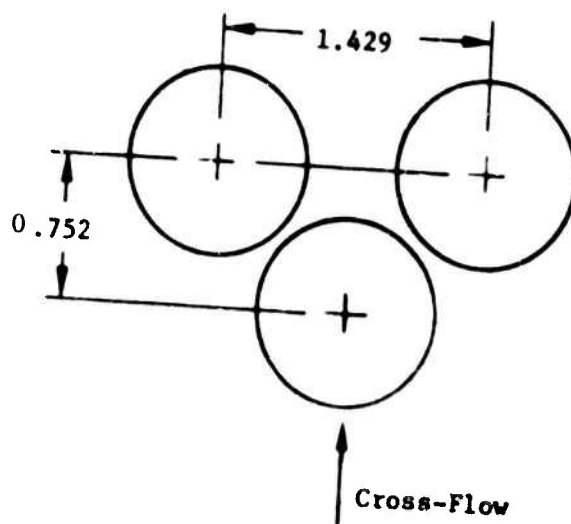
Figure 8. Profiles of M-117 Bomb Shapes



(a) Single Body



(b) Two Body



(c) Three Body

NOTE: All dimensions in
body diameters

Figure 9. Single and Multiple Body Configurations (Carriage Position)

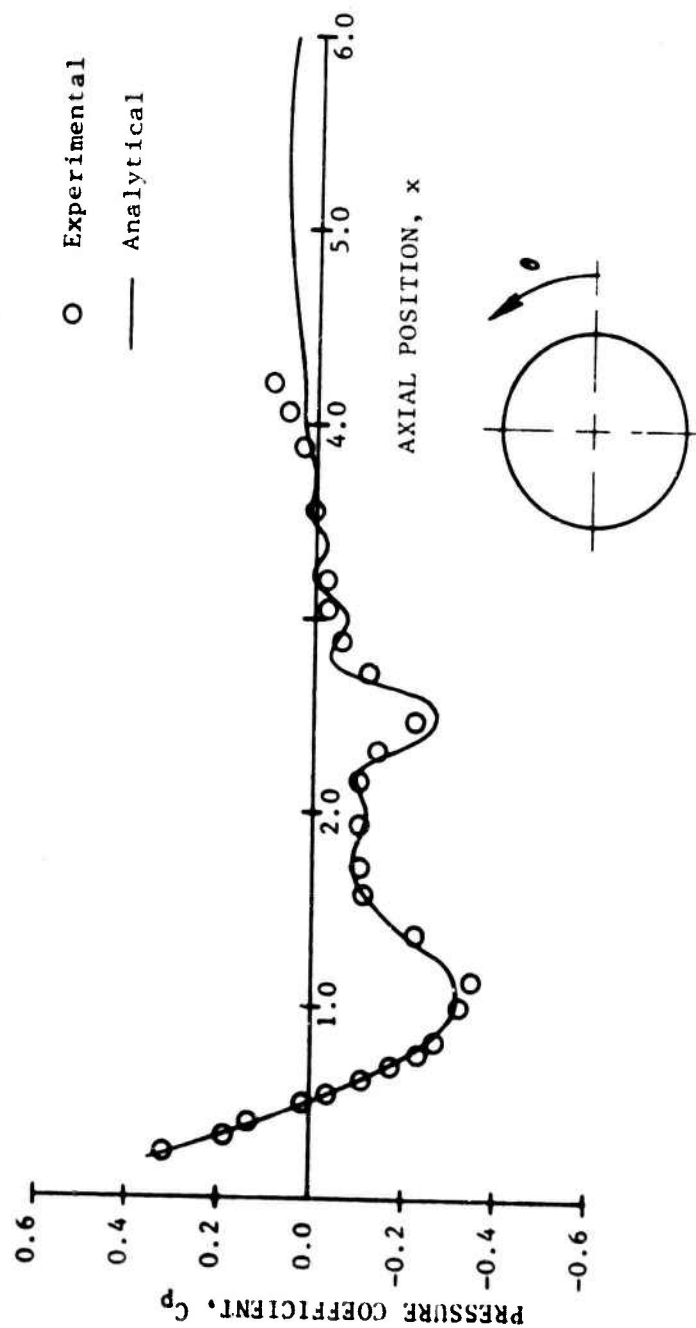


Figure 10. Pressure Distribution - Single Body at 0-Degree Angle of Attack ($\theta=0^\circ$)

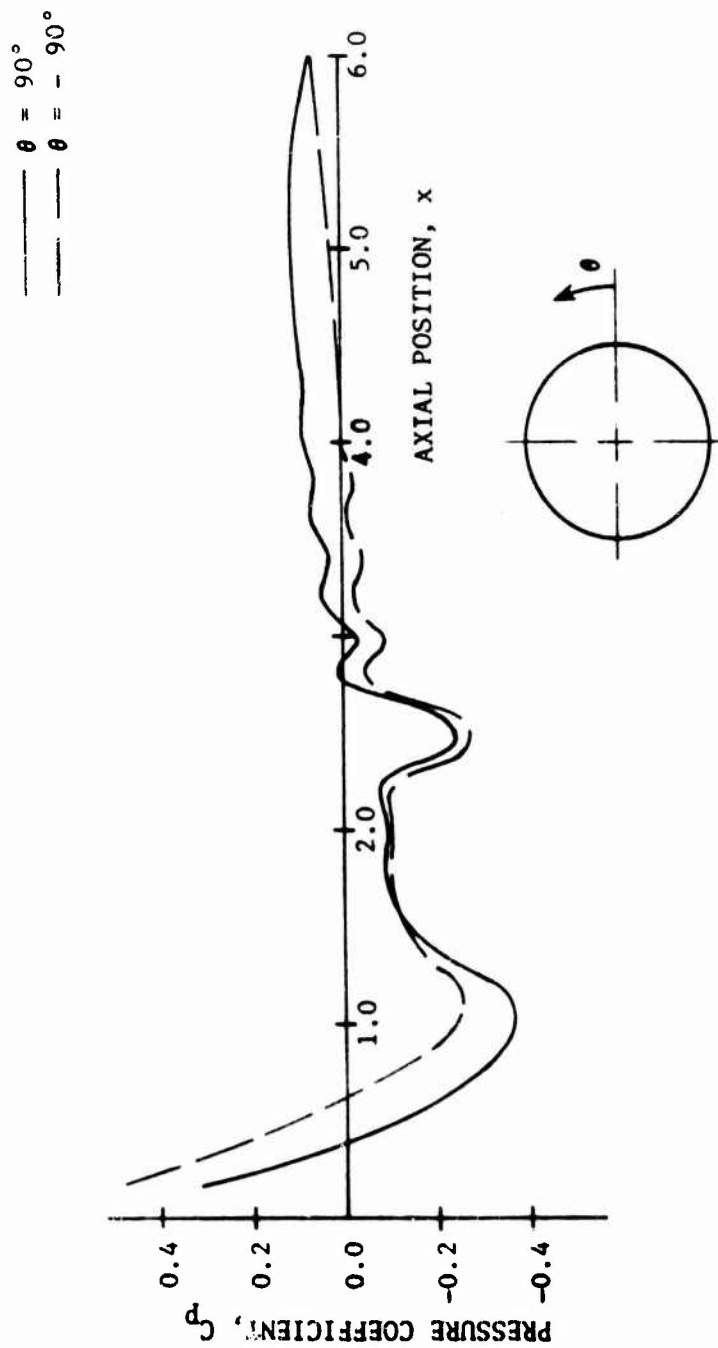


Figure 11. Pressure Distribution - Single Body at 5-Degree Angle of Attack

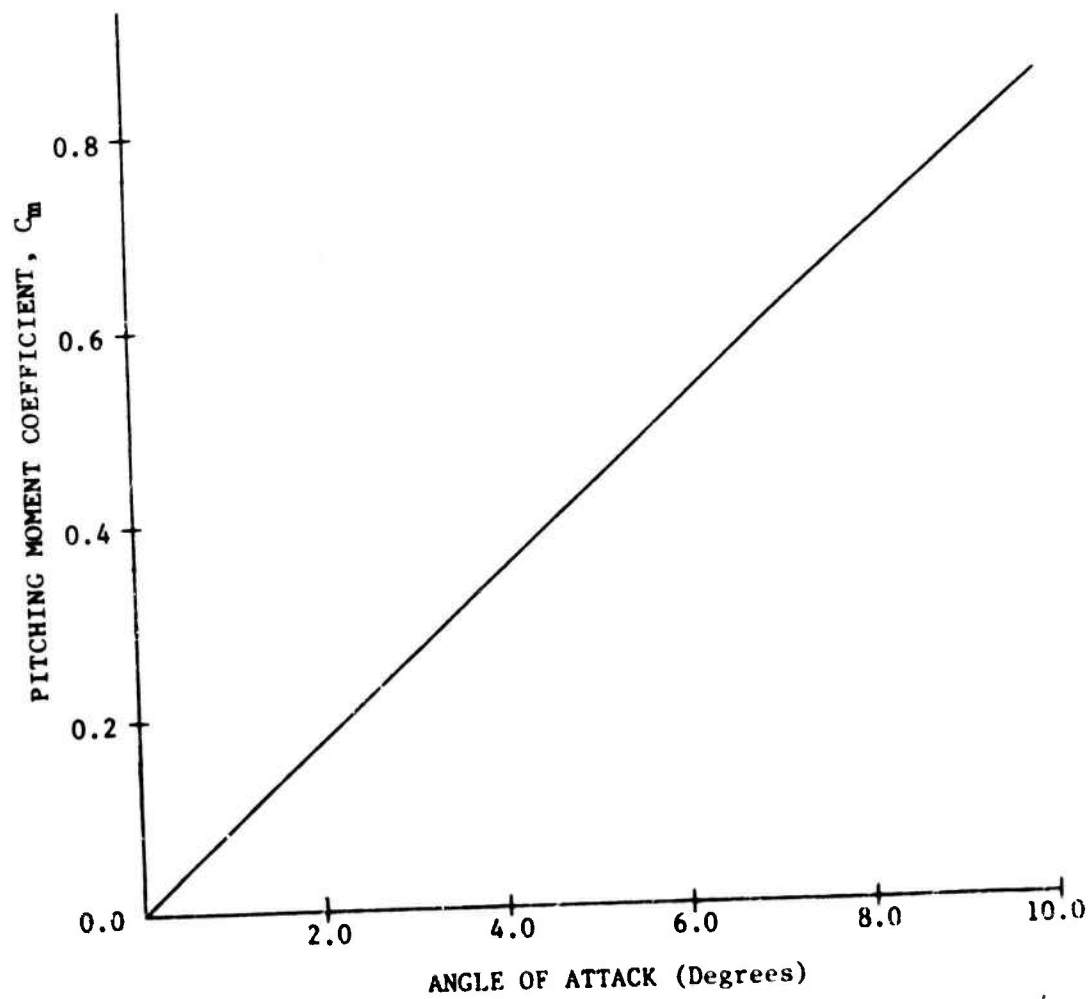


Figure 12. Pitching Moment Coefficient - Single Body

Error calculations for a single body at angle of attack showed that the difference between the inclination of the streamlines at the body surface for points in meridian planes other than that containing the control points and the inclination of the actual body surface did not exceed 0.0005 degree at any of the points checked.

TWO PARALLEL BODIES

The case of two parallel M-117 bombs aligned with the flow was treated in Reference 2. As in Reference 2, the distance between the center lines of two bodies used for this case is 1.042 diameters. This corresponds to the separation of two M-117 bombs when mounted on a Triple Ejector Rack (TER). The resulting pressure distribution was found to be in good agreement with experiment as shown in Figures 13 and 14. No experimental data are available for this two-body case at an angle of attack; however, the relative change in the pressure distributions is shown in Figure 15. As can be seen from this figure, the pressure coefficient at the point between the bodies, $\theta=180$ degrees, is apparently insensitive to the angle of attack. However, there does seem to be a significant change with angle of attack at $\theta=0$ degrees. The effect of angle of attack on side force and pitching moment coefficients is shown in Figures 16 and 17.

To explore the validity of this image system a check was made on the body boundary conditions at meridian planes other than that containing the control points. The poorest match of the tangent flow boundary condition occurred along the outside meridian and the magnitude of the error incurred was unaffected by the angle of attack. A plot of the difference between the body surface angle and the flow angle along this meridian is shown in Figure 18.

THREE BODIES

The three body case represents three M-117 bombs in their relative positions as if mounted on a TER and is shown in Figure 9(c). Experimental data for this configuration at zero angle of attack were obtained from a pressure model and two models of the M-117 bomb in the low-speed wind tunnel of the contractor. The results of the wind tunnel test and theory for the top meridional plane of the central body are shown in Figure 19. As can be seen, the agreement between theory and experiment is poor along the aft portion of the body. Subsequent wind tunnel tuft tests have shown that there is flow separation between the bodies along the tails of all three bodies. It was for this reason that it was decided to analytically modify the shape of the M-117 to try to account for flow separation along one side on the tail of the body.

The non-axisymmetric configuration considered consists of the normal M-117 nose and center sections. The tail section, however, has a decreased taper and angled centerline such that one side maintains the original contour of the M-117 tail while the opposite side is displaced [See Figure 8(b)]. All three bodies were modified in this manner with the tail of the central body being warped upward and the tails of the two upper bodies being warped toward the central body. The center line of the tail of the modified body was set at an angle of 2 degrees. The pressure distribution

obtained for this case along the top meridian of the central body is shown in Figure 20, and at least indicates a trend toward improvement in the agreement between experiment and theory in the tail region.

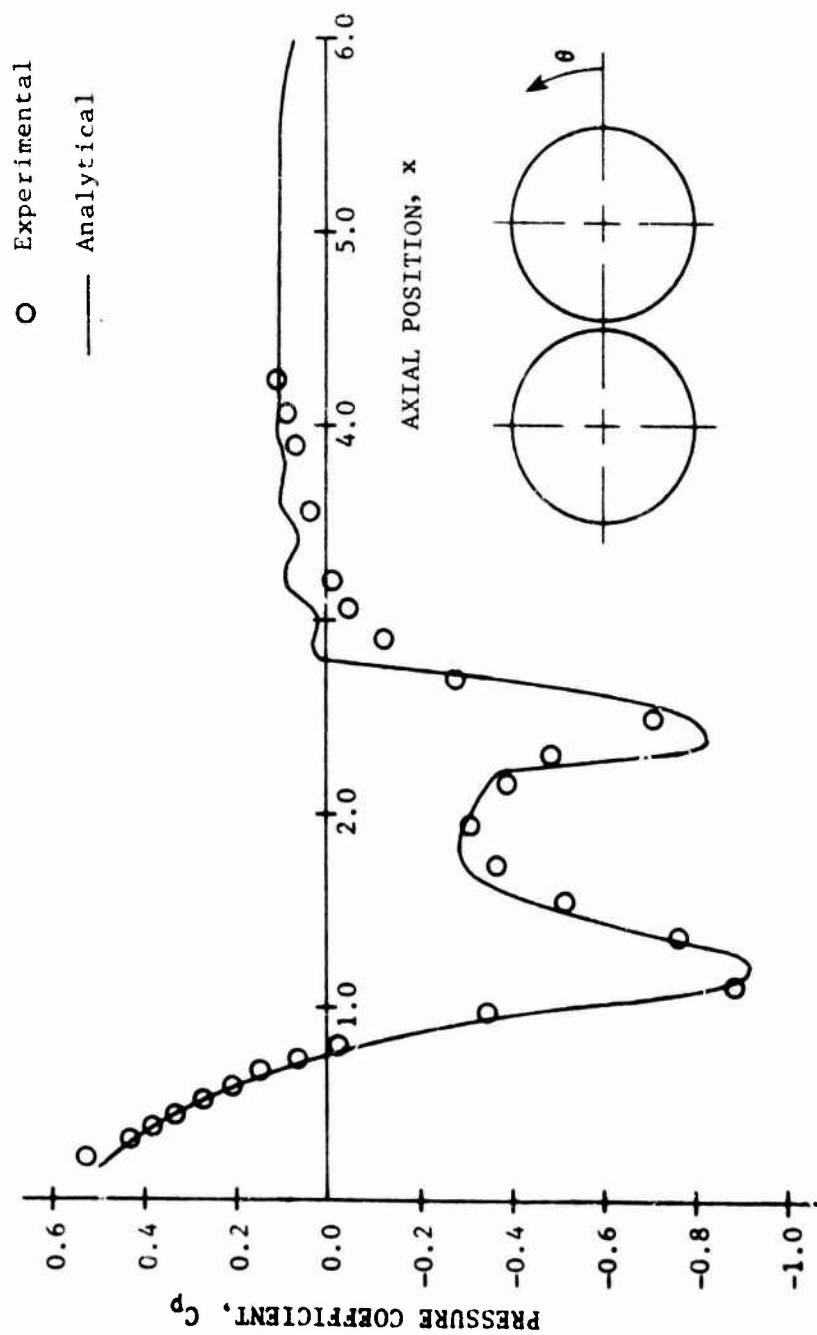


Figure 13. Pressure Distribution - Two Bodies at 0-Degree Angle of Attack ($\theta=180^\circ$)

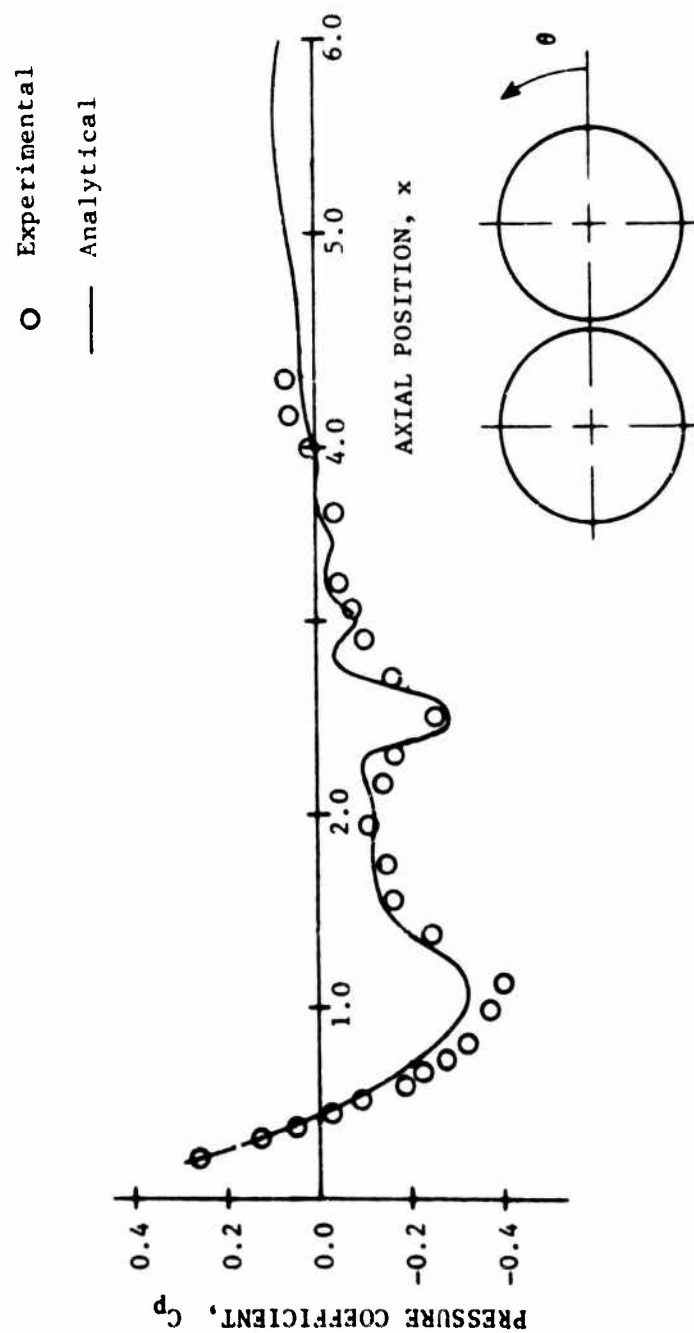


Figure 14. Pressure Distribution - Two Bodies at 0-Degree Angle of Attack ($\theta=0^\circ$)

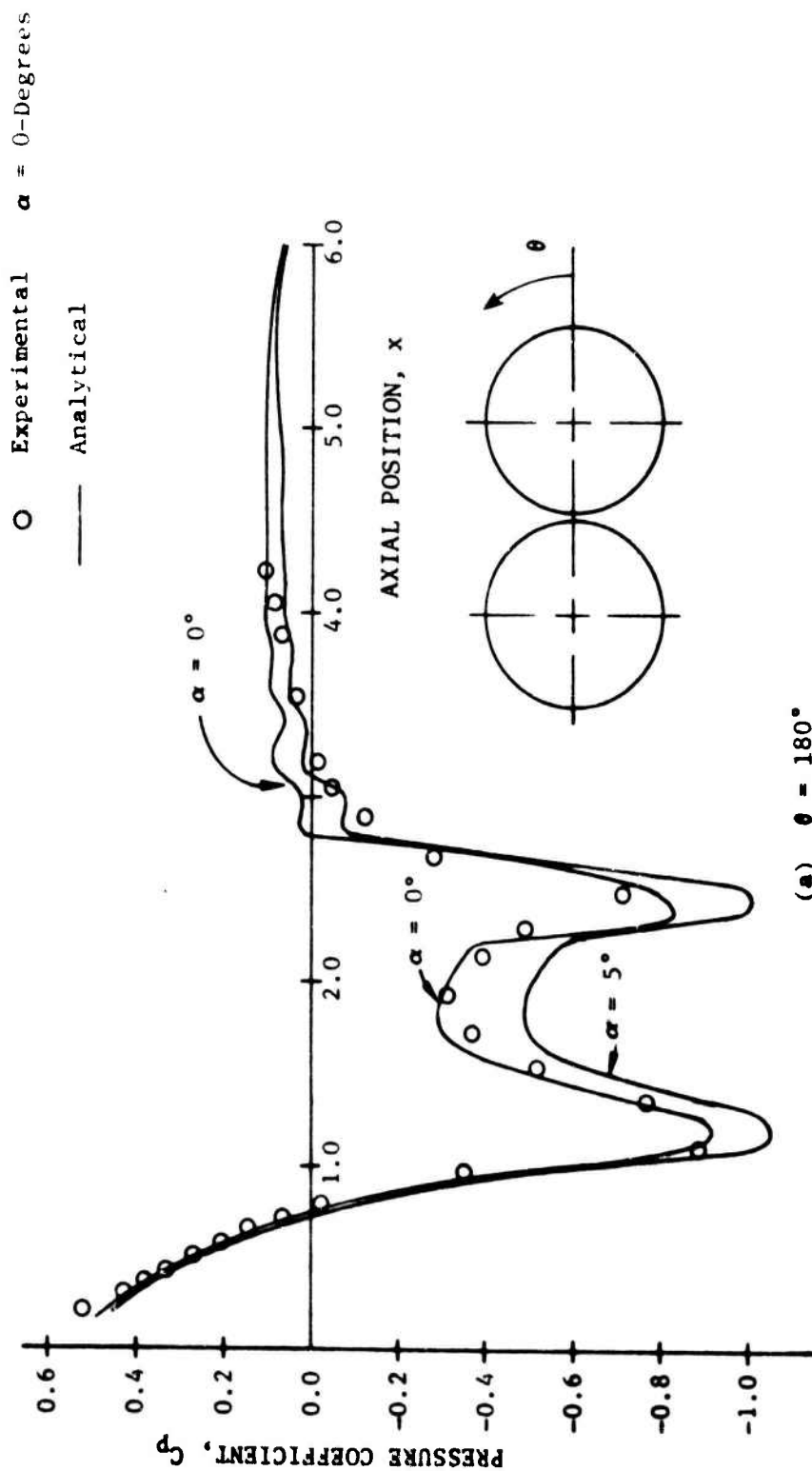
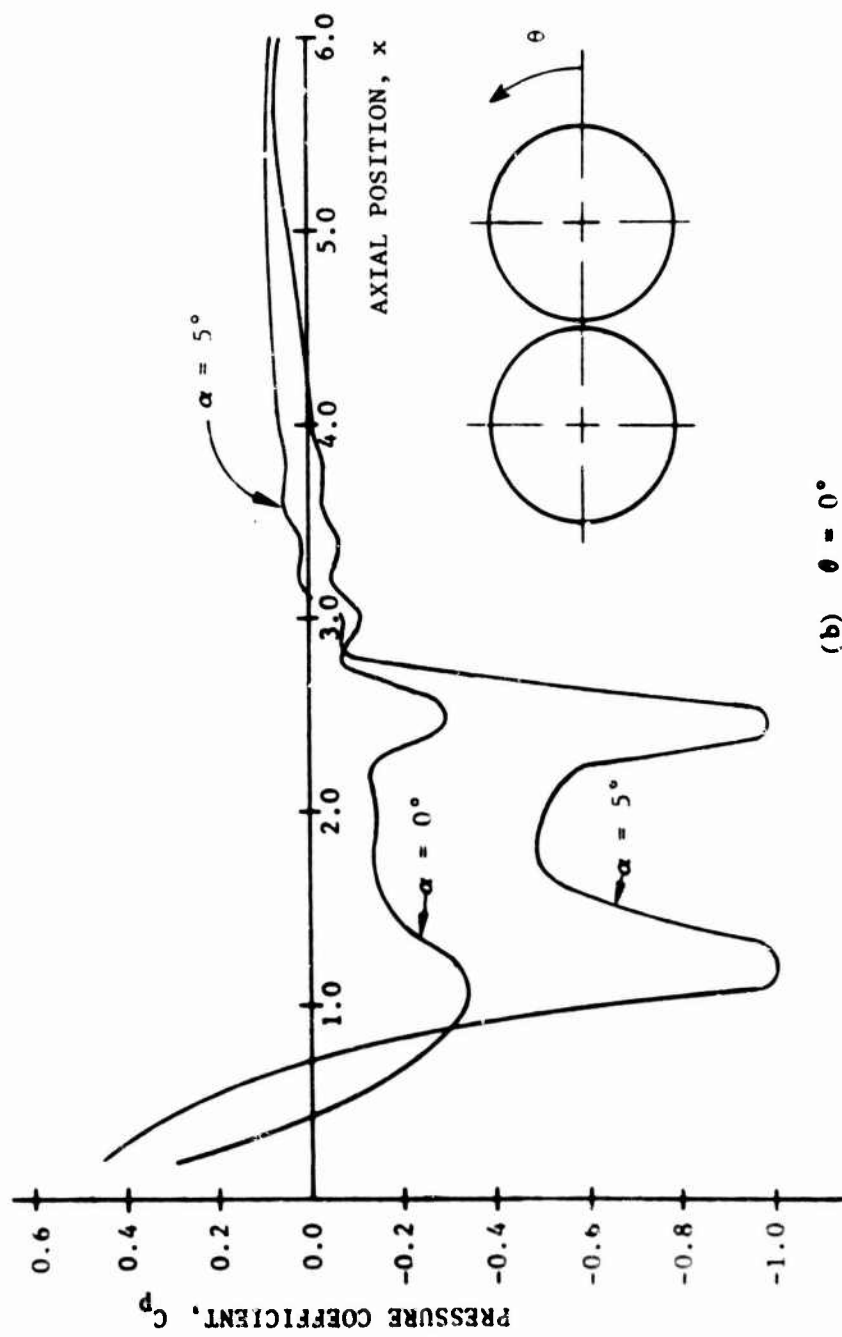


Figure 15. Comparison of the Analytical Pressure Distributions for Two Bodies at 0- and 5-Degree Angle of Attack



(b) $\theta = 0^\circ$

Figure 15. Comparison of the Analytical Pressure Distribution for Two Bodies at 0- and 5-Degree Angle of Attack (Concluded)

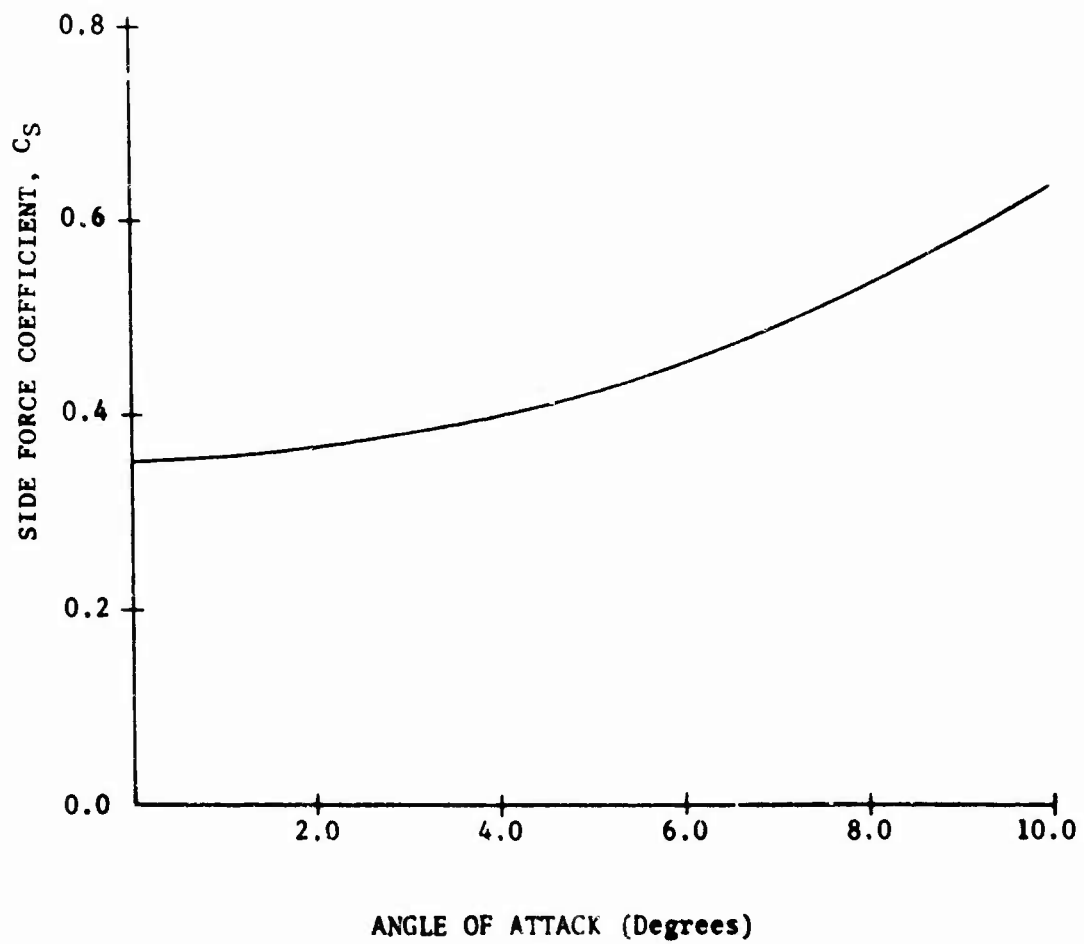


Figure 16. Side Force Coefficient - Two Body Configuration

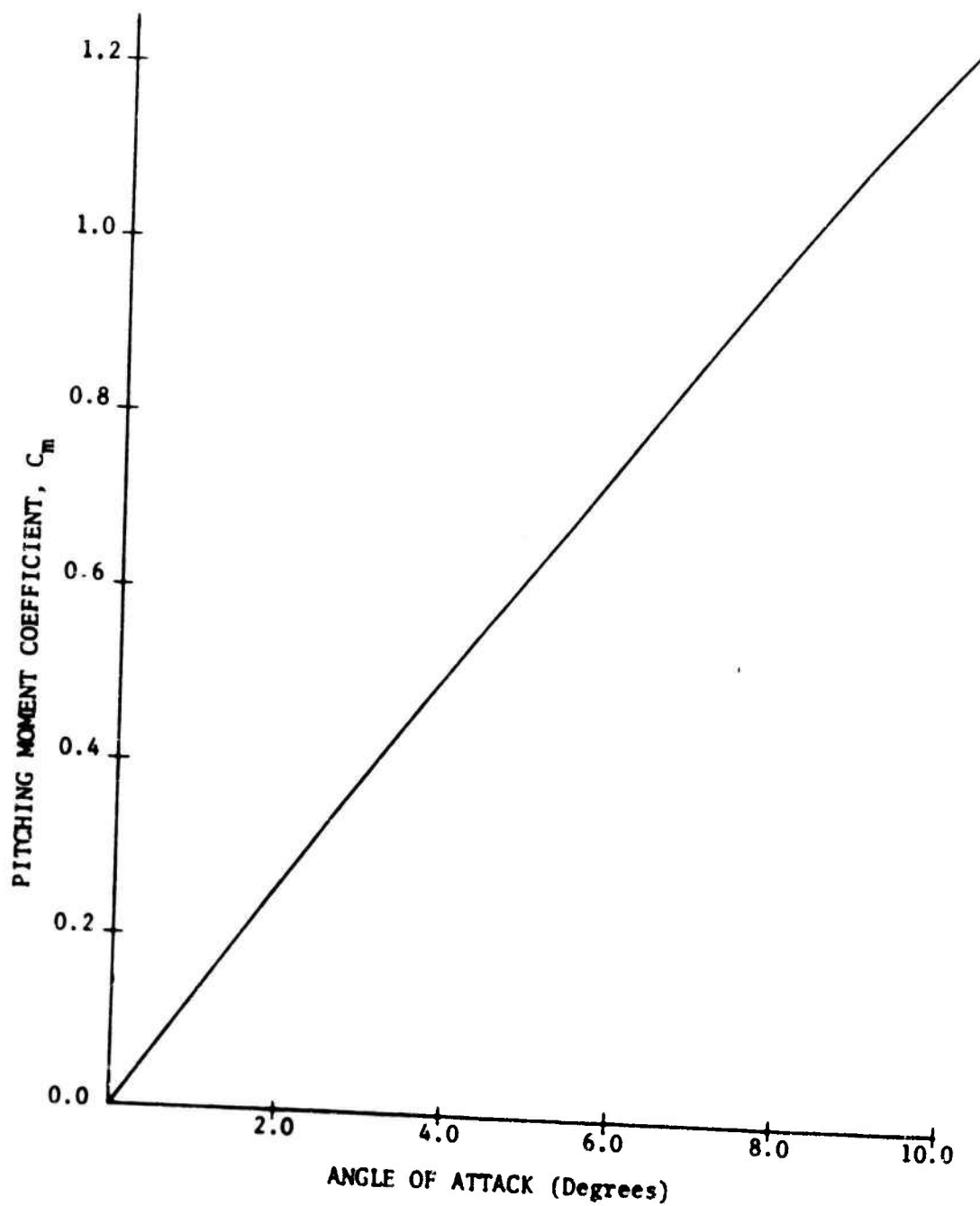


Figure 17. Pitching Moment Coefficient - Two Body Configuration

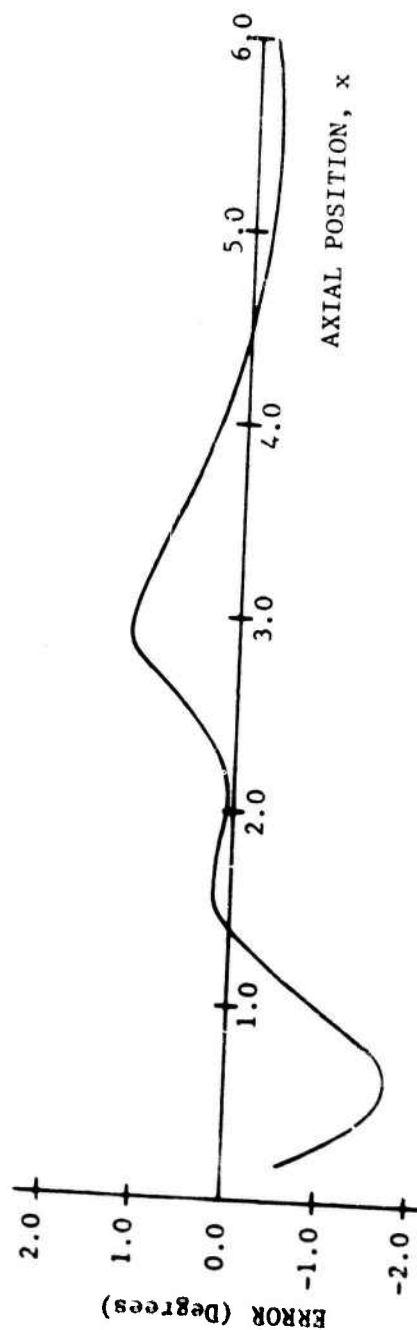


Figure 18. Boundary Condition Error Distribution - Two Bodies ($\theta=0^\circ$)

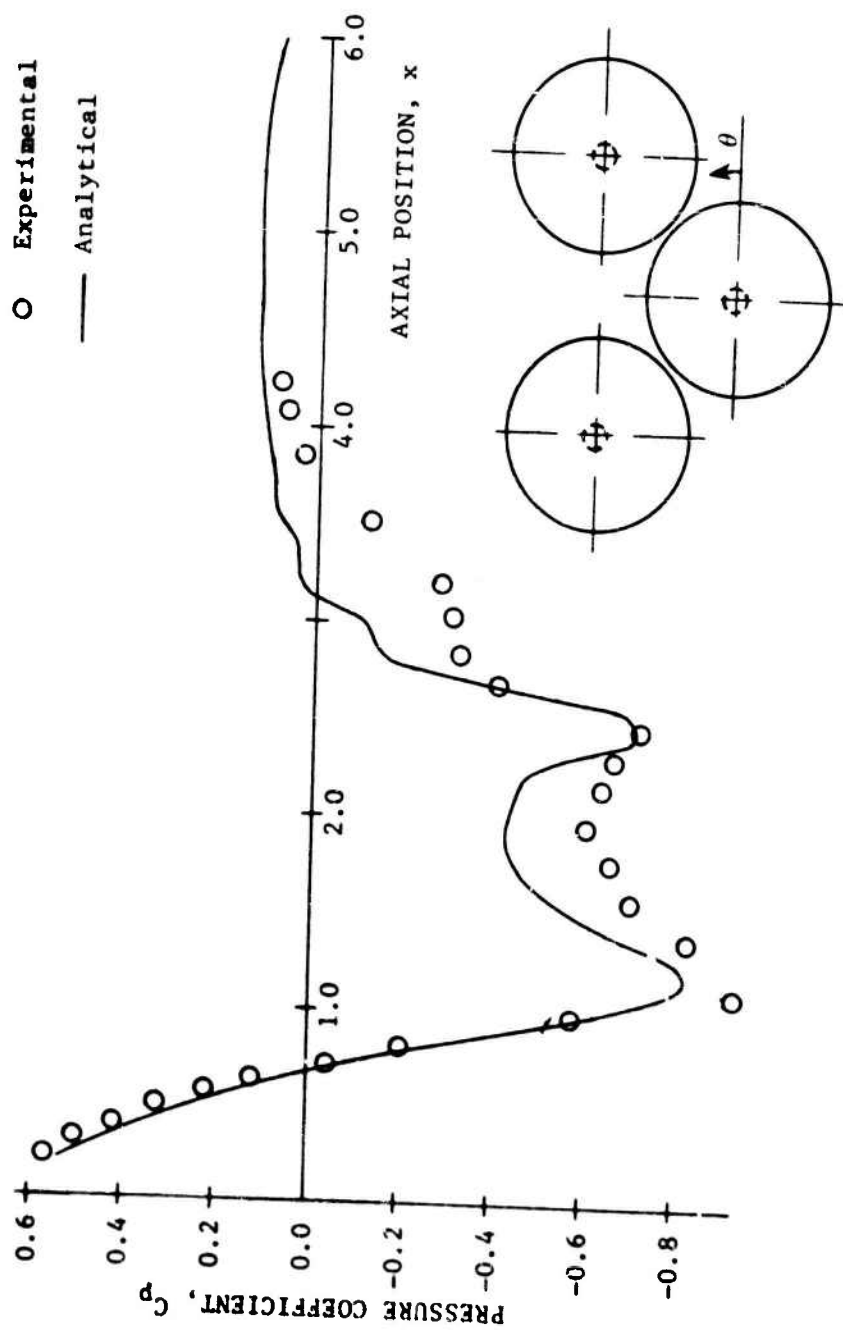


Figure 19. Pressure Distribution - Three Axisymmetric Bodies ($\theta=90^\circ$)

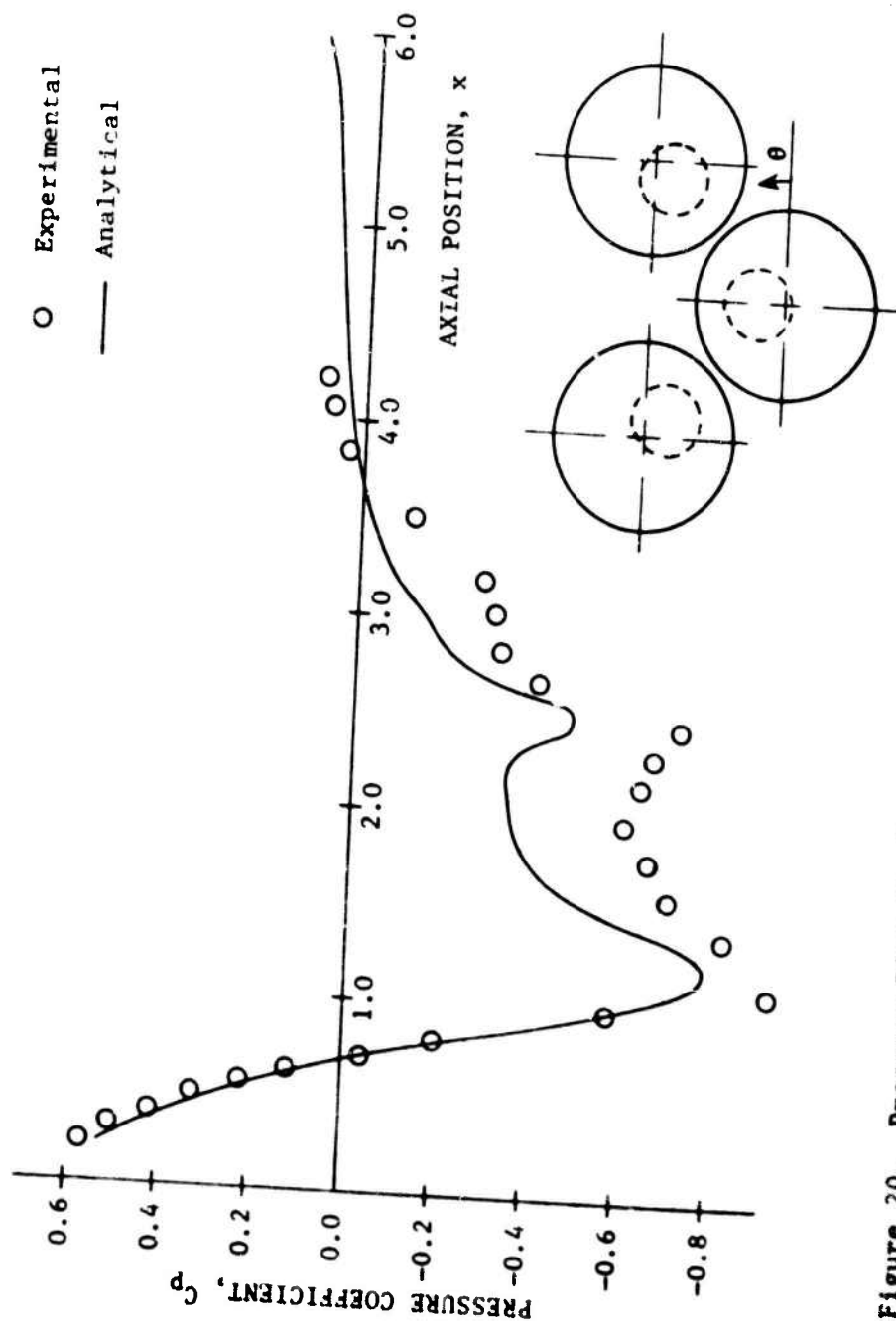


Figure 20. Pressure Distribution - Three Modified Non-Axisymmetric Bodies ($\theta=90^\circ$)

SECTION IV

CONCLUSIONS

The force and moment coefficients plotted in the numerical examples show significant variation with angle of attack; linear in the case of two-body pitching moment, nonlinear in the case of two-body side force. This indicates that for complete investigation of interference effects the freestream cross-flow due to angle of attack should be taken into account.

The modification of body geometry to account for flow separation was found to be inadequate for the particular case tried in the numerical examples. It was found, however, that some of the characteristics of the separated flow were simulated by the distorted body and it is speculated that this method might be used successfully for flow separation problems that are less complex than the one tried in the numerical examples.

It is also suggested that the capability of modeling slightly non-axisymmetric bodies will be useful for many flow problems. One foreseen application of this technique is the representation of the flow field in the vicinity of an aircraft fuselage by using multiple non-axisymmetric bodies that approximate the shape of the fuselage.

APPENDIX A

INFLUENCE COEFFICIENTS

Source Flow

The potential function of a three-dimensional source as given in Section 15-20 of Reference 4 is $\phi = m/r$ (reversing the sign convention results in $\phi = -m/r$). This function can be described in a three-dimensional coordinate system with the source located at the origin by letting $r = (x^2+y^2+z^2)^{1/2}$; therefore

$$\phi = \frac{-m}{(x^2+y^2+z^2)^{1/2}} \quad (\text{A-1})$$

The velocities in the x, y, and z directions that are induced by the source at the point (x,y,z) can be found by the partial differentiation of the field potential:

$$U_x = \frac{\partial \phi}{\partial x} = m \frac{x}{\{x^2+y^2+z^2\}^{3/2}} \quad (\text{A-2})$$

$$U_y = \frac{\partial \phi}{\partial y} = m \frac{y}{\{x^2+y^2+z^2\}^{3/2}} \quad (\text{A-3})$$

$$U_z = \frac{\partial \phi}{\partial z} = m \frac{z}{\{x^2+y^2+z^2\}^{3/2}} \quad (\text{A-4})$$

The velocity influence coefficients, C_{x_s} , C_{y_s} , and C_{z_s} are defined as

$$C_{x_s} \equiv \frac{U_x}{m} \quad (\text{A-5})$$

$$C_{y_s} \equiv \frac{U_y}{m} \quad (\text{A-6})$$

and

$$C_{z_s} \equiv \frac{U_z}{m} \quad (\text{A-7})$$

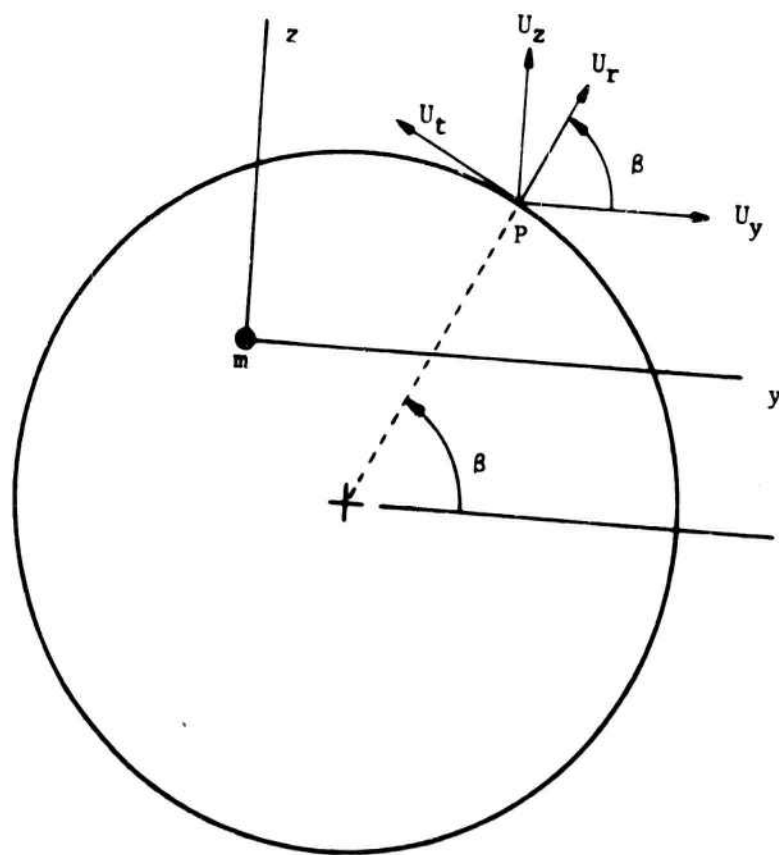


Figure A-1. Transformation of Induced Velocities

Therefore, using Equations (A-2, A-3, and A-4), then

$$C_{x_s} = \frac{x}{\{x^2+y^2+z^2\}^{3/2}} \quad (A-8)$$

$$C_{y_s} = \frac{y}{\{x^2+y^2+z^2\}^{3/2}} \quad (A-9)$$

$$C_{z_s} = \frac{z}{\{x^2+y^2+z^2\}^{3/2}} \quad (A-10)$$

Doublet Flow

The potential function of a three-dimensional doublet of strength μ is given in Section 15.26 of Reference 4 (after sign reversal again) as

$$\phi = -\mu \frac{\cos \theta}{r^2}$$

If the doublet is considered at the origin of an x, y, z axis system with the doublet axis oriented in the negative y direction, then r becomes $(x^2+y^2+z^2)^{1/2}$, $\cos \theta$ becomes $-y/(x^2+y^2+z^2)^{1/2}$ and the velocity potential becomes

$$\phi = \frac{\mu y}{(x^2+y^2+z^2)^{3/2}} \quad (A-11)$$

Differentiating Equation (A-11) yields the velocity components:

$$U_x = \frac{\partial \phi}{\partial x} = \frac{-3xy}{(x^2+y^2+z^2)^{5/2}} \mu \quad (A-12)$$

$$U_y = \frac{\partial \phi}{\partial y} = \left\{ \frac{1}{(x^2+y^2+z^2)^{3/2}} - \frac{3y^2}{(x^2+y^2+z^2)^{5/2}} \right\} \mu \quad (A-13)$$

$$U_z = \frac{\partial \phi}{\partial z} = \frac{-3zy}{(x^2+y^2+z^2)^{5/2}} \mu \quad (A-14)$$

The velocity influence coefficients of the doublet are defined as

$$C_{x_d} = \frac{U_x}{\mu} \quad (A-15)$$

$$C_{y_d} = \frac{U_y}{\mu} \quad (A-16)$$

$$C_{z_d} = \frac{U_z}{\mu} \quad (A-17)$$

Using Equations (A-12, A-13, and A-14), then

$$C_{x_d} = \frac{-3xy}{(x^2+y^2+z^2)^{5/2}} \quad (A-18)$$

$$C_{y_d} = \frac{1}{(x^2+y^2+z^2)^{3/2}} - \frac{3y^2}{(x^2+y^2+z^2)^{5/2}} \quad (A-19)$$

$$C_{z_d} = \frac{-3zy}{(x^2+y^2+z^2)^{5/2}} \quad (A-20)$$

Transformation

The velocity coefficients, of course, can be transformed into another coordinate system if desired. For example, if a source of strength m is located inside of a circle as shown in Figure A-1, with the x axis pointing into the paper, then the radial and tangential velocities (U_r and U_t) induced by the source m , at the point, P , can be found by transforming the velocity components in the y and z directions through the angle β . This gives

$$U_r = U_y \cos \beta + U_z \sin \beta \quad (A-21)$$

$$U_t = U_z \cos \beta - U_y \sin \beta \quad (A-22)$$

Using the velocity influence coefficients as previously derived, then,

$$U_r = C_{y_s} m \cos \beta + C_{z_s} m \sin \beta \quad (A-23)$$

$$U_t = C_{z_s} m \cos \beta - C_{y_s} m \sin \beta \quad (A-24)$$

Defining the radial and tangential velocity influence coefficients of the source as

$$C_{r_s} \equiv \frac{U_r}{m} \quad \text{and} \quad C_{t_s} \equiv \frac{U_t}{m}, \quad \text{then}$$

$$C_{r_s} = C_{y_s} \cos \beta + C_{z_s} \sin \beta \quad (\text{A-25})$$

and

$$C_{t_s} = C_{z_s} \cos \beta - C_{y_s} \sin \beta \quad (\text{A-26})$$

Comparing Equations (A-25 and A-26) with Equations (A-21 and A-22), it can be seen that the velocity influence coefficients can be transformed as if they were actual velocities.

APPENDIX B

IMAGE SYSTEM FOR TWO CIRCULAR CROSS-SECTIONS IN TWO-DIMENSIONAL FLOW

The problem discussed here has been previously treated in Section IV of Reference 1 and is discussed here as an aid to the reader.

From the single body solution for an axisymmetric body, there exist a number of point sources located along the body's axis that are used to satisfy the tangent flow boundary condition at the body surface. If two such mathematical models are brought into close proximity, then the sources in each body will create perturbations at the other body's surface and therefore will be mutual distortion of the body shapes. A two-dimensional approach is taken to find an appropriate image system that will preserve the body shapes.

A cross-section of the two bodies is represented in two-dimensional flow by two circles with a source at each center as shown in Figure B-1. It is desired that the circular shape of Body A be maintained by creating an image system that will cancel the perturbations induced by the source in Body B that are normal to the surface of Body A. The image (derived in Section 8.61 of Reference 4) for a source outside of a circular cylinder satisfies this condition. Therefore, the image system required consists of a sink of strength m_b at the center of A and a source of equal strength displaced from the center of A toward the center of B by an amount a^2/f where a is the radius of A and f is the distance between the centers of A and B.

An image system is also desired in B to counteract the source of A. This will consist of a sink of strength m_a at the center of B and a source of equal strength displaced from the center of B toward the center of A by an amount b^2/f where b is the radius of B (See Figure B-2).

Additional images are now needed in A and B to counteract the effects of the additional sources and sinks added to A and B. That is, a sink of strength m_a at the center of A and a source of equal strength displaced a distance $a^2/(f-b^2/f)$ from the center of A are needed to counteract the effect of the image source in B. Also, a source of strength m_a at the center of A and a sink of equal magnitude displaced from the center of A by an amount a^2/f are needed to counteract the effects of image sink in B. A similar situation is found in B. After these images are added, then additional images are needed for them also, and so on to infinity. Figure B-3 shows the results of several iterations.

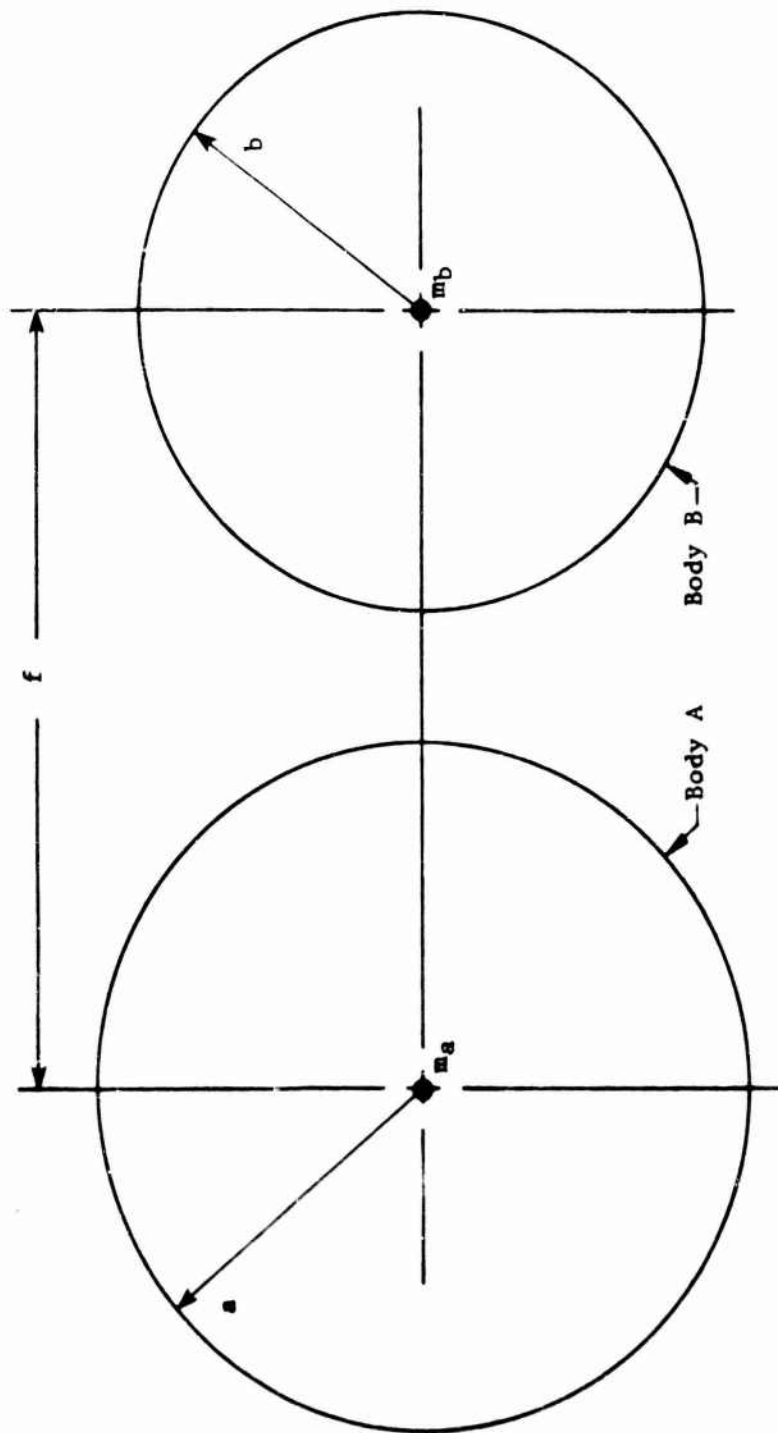


Figure B-1. Two-Dimensional Representation of a Cross-Section of Two Bodies
(without image system)

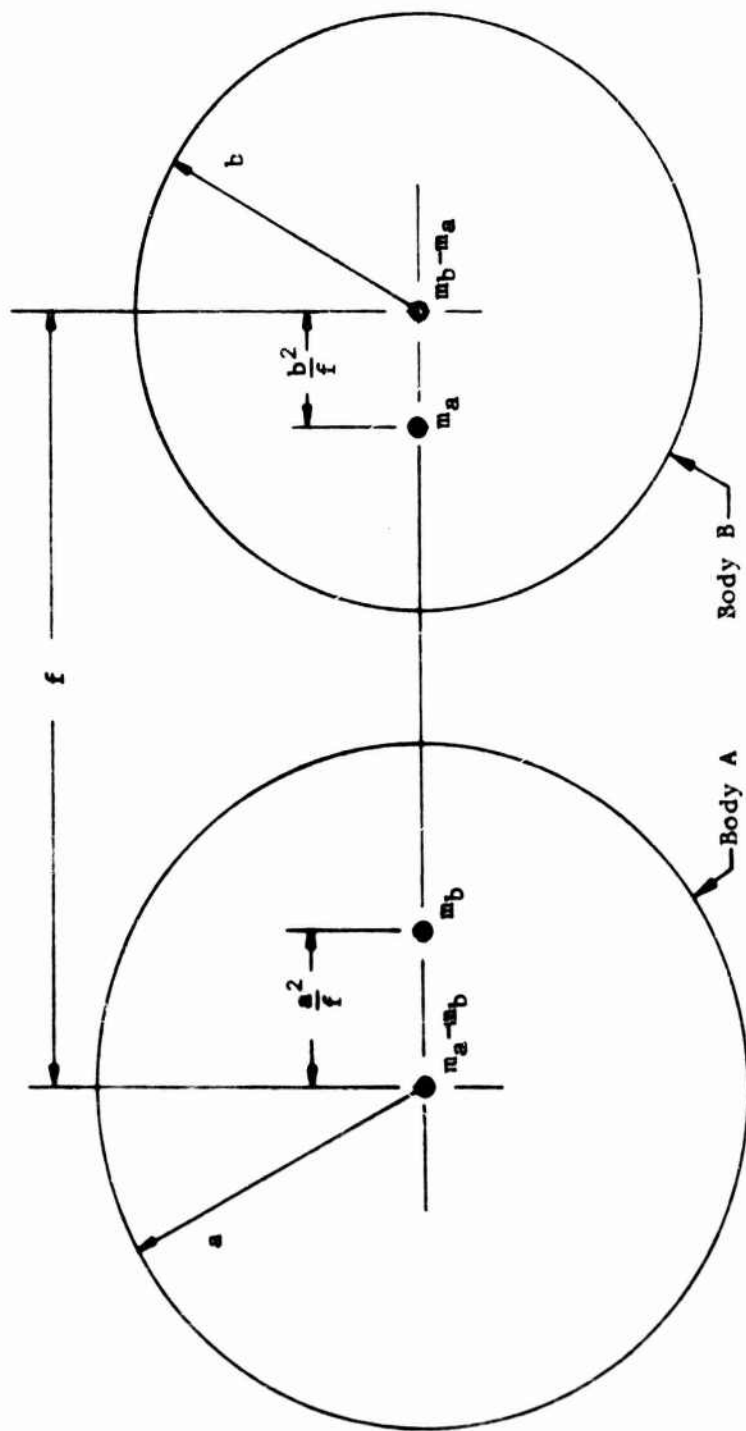


Figure B-2. Two Circles with the First Iteration of Image System

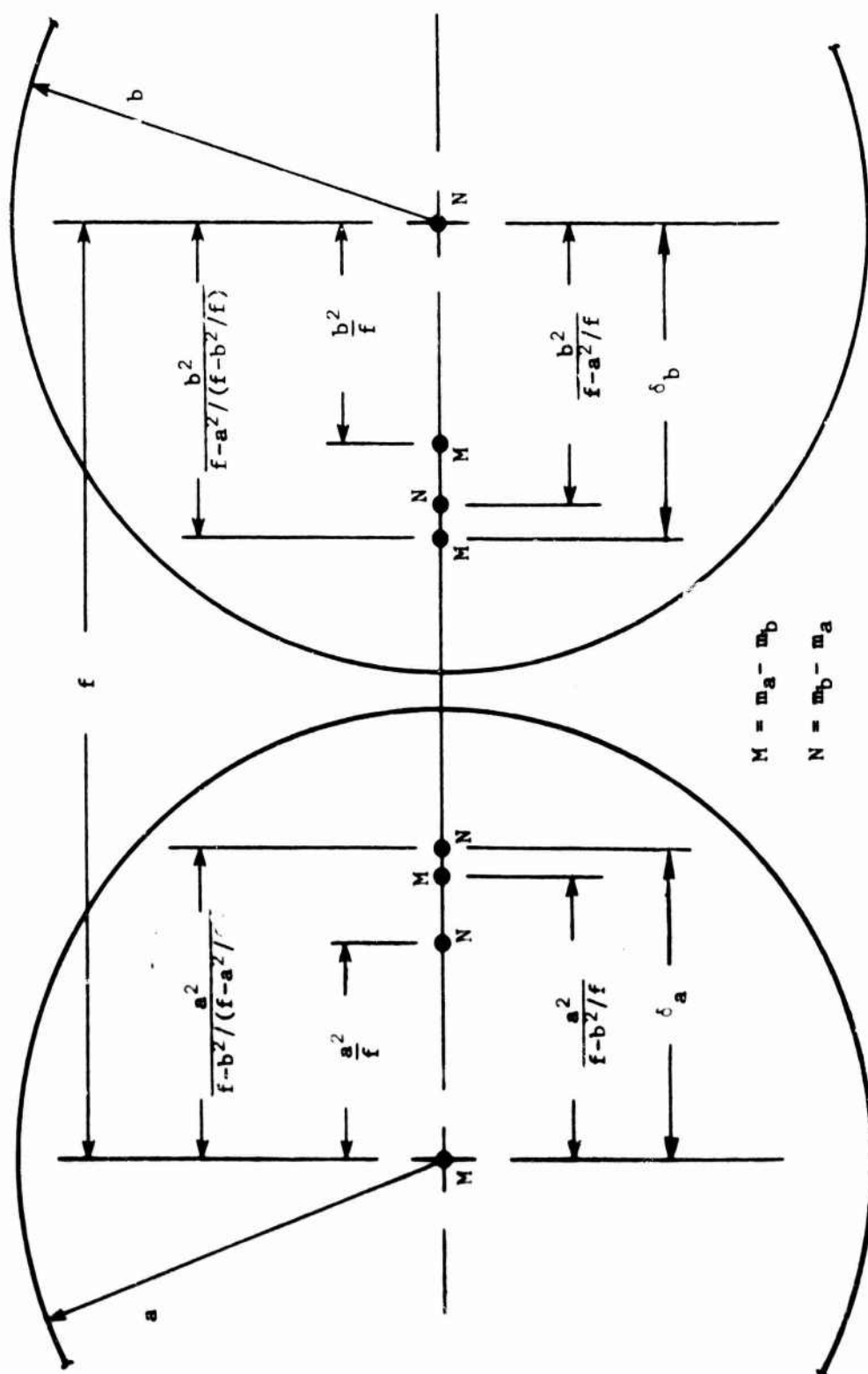


Figure B-3. Two Circles with Third Iteration of Image System

The displacement of the sources from the center of the circle reaches a limiting point (See Figure B-3) and the displacement of the infinite iteration is expressed as (using the displacement in circle A as an example)

$$\delta = a^2 / (f - b^2 / (f - a^2 / (f - b^2 / (f - a^2 / (\dots)))))) \quad (B-1)$$

Examining Equation (B-1), it can be seen that due to the infinite series the equation can be rewritten as

$$\delta = \frac{a^2}{f - \frac{b^2}{f - \delta}} \quad (B-2)$$

Rearranging Equation (B-2), it can be seen that

$$\delta^2 - \left[f - \frac{(b^2 - a^2)}{f} \right] \delta + a^2 = 0 \quad (B-3)$$

Solving the quadratic equation for δ ,

$$\delta = \frac{1}{2} \left[f - \frac{b^2 - a^2}{f} \right] - \left\{ \frac{1}{4} \left[f - \frac{b^2 - a^2}{f} \right]^2 - a^2 \right\}^{1/2} \quad (B-4)$$

(The solution with a positive radical lies outside the circle and is therefore not considered).

A similar solution can be found for the limit of the displacement in B and the result is the same as Equation (B-4) except that a and b are switched.

REFERENCES

1. Martin, Fred W.: Mutual Aerodynamic Interference Effects by the Cross-Flow Corrections Method. AFATL-TR-71-69, June, 1971.
2. Martin, Fred W., Smith, Charles J., and Saunders, Grady H., Jr.: Mutual Aerodynamic Interference Effects for Two Axisymmetric Bodies. AFATL-TR-73-161, August, 1973.
3. Angelucci, Silvio B.: "A Multivortex Method for Axisymmetric Bodies at Angle of Attack.: Journal of Aircraft, Vol. 8, No. 12, December, 1971, p. 959.
4. Milne-Thomson, L.M.: Theoretical Hydrodynamics. The MacMillan Company, third edition, 1957.
5. Mattasits, G.R.: Aerodynamic Interference Effects on Various Weapon Shapes in the Flow Field of a Transonic Wing Configuration at Mach Numbers from 0.5 to 1.3. AEDC-TR-75-92, AFATL-TR-75-88, July 1975.

LIST OF SYMBOLS

a	Local radius of Body A
A	Denotes Circle A or Body A
b	Local radius of Body B
B	Denotes Circle B or Body B
C_m	Pitching moment coefficient
C_p	Pressure coefficient
C_r	Radial velocity influence coefficient (at a control point)
C_s	Side force coefficient
C_x	Axial velocity influence coefficient (at a control point)
f	Distance between the centers of two circles
m	Source strength (τ_i is strength of i^{th} source)
N_s	Number of stations along body
R	Radius of body cross-section
R_w	Displacement of body centerline
S	Slope of body surface with respect to centerline
U_r	Radial velocity
U_x	Axial velocity
\bar{V}	Velocity vector
w	Complex potential function
x, y, z	Rectangular coordinates (x along body)
Y_o	Distance between centerline of Body A and Body B measured perpendicularly to centerline of Body A

LIST OF SYMBOLS (CONTINUED)

Z	Complex coordinates
β	Transformation Angle
δ	Source displacement distance
η	Orientation of doublet axis
θ	Angular coordinate
μ	Doublet strength
ϕ	Velocity potential
ϕ_w	Angular location of displacement of body centerline
ψ_w	Rotation of body cross-section due to displacement of body centerline
∇^2	Laplacian operator
●	Source location
⚡	Doublet Location

LIST OF SYMBOLS (CONCLUDED)

Subscripts

- a Denotes a relationship with Body A
- b Denotes a relationship with Body B
- d Indicates a property associated with a doublet
- i,k Refers to the i^{th} source or the i^{th} doublet or i^{th} body or k^{th} body.
- p Denotes a property associated with image pairs
- v Denotes radial property or value
- s Indicates a property associated with a source
- t Indicates tangential property or value
- x Denotes axial property or value
- ∞ Denotes freestream value
- δ Denotes property associated with displaced or image doublets

Superscripts

- + Indicates property associated with source
(+ implied if omitted)
- Indicates property associated with sink

INITIAL DISTRIBUTION

USAF/RDQRM	2
AFSC/SDWM	1
AFSC/DLCAW	1
FL2302, Tech Lib, 2750ABW/SSL	1
Ogden ALC/MMNOP	1
AFIS/INTA	2
AFWL/LR	1
AUL (AUL/LSE-70-239)	2
CO, NATC, CT-17, TID/Tech Pubs	1
Redstone Sci Info Cntr/Doc Sec	2
Nav Ord Stn/Tech Lib	2
Nav Surface Wpns Cntr/Tech Lib	1
CO, USNWC (Code 533)	2
Dir, Nav Research Lab (Code 7785)	1
Sandia Lab/Tech Lib Div 3141	1
DDC	1
AFATL/DLOSL	2
AFATL/DL	2
AFATL/DLJ	1
AFATL/DLJC	1
TAWC/TRADOCLO	1
AFFDL/FGC	1
ASD/ENFEA	1
USAF (AF/SAMI)	1
ASD/ENYEHM	1
AFFTC, 6510 ABGP/SSD, Tech Lib	1
AFIT/LD	1
AEDC (ARO, Inc)	1
CO, USNWC (Code 4063)	1
Nav Ship R&D Cntr (Code 166/Acft Div)	1
AFATL/DLJA	1